UNIVERSITY OF CALIFORNIA

Los Angeles

Aspects of Highly-Correlated Electron Systems

A dissertation submitted in partial satisfaction

of the requirements for the degree

Doctor of Philosophy in Physics

by

Nicholas Demetrios Rombes III

2020

ABSTRACT OF THE DISSERTATION

Aspects of Highly-Correlated Electron Systems

by

Nicholas Demetrios Rombes III
Doctor of Philosophy in Physics
University of California, Los Angeles, 2020
Professor Sudip Chakravarty, Chair

We begin by scrutinizing a recent proposal that presents an alternate description of the half-filled Landau level in terms of massless Dirac fermions. In Chapter 2, we examine the possibility of pairing of these Dirac fermions by numerically solving the coupled Eliashberg equations unlike a related previous calculation (Wang and Chakravarty, 2016). In addition, vertex corrections are calculated to be zero from the Ward identity. We find that pairing is possible in non-zero angular momentum channels; only differences are minor numerical shifts. As before, the pairing leads to the gapped Pfaffian and anti-Pfaffian states. However, in our approximation scheme, pairing is not possible in the putative particle–hole symmetric state for $l = 0$ angular momentum. The specific heat at low temperatures of a system of massless Dirac fermions interacting with a transverse gauge field, expected to be relevant for the half-filled Landau level, is calculated. Using the Luttinger formula, it is found to be $\propto T \ln T$ in the leading low temperature limit, due to the exchange of transverse gauge bosons. The result agrees with the corresponding one in the nonrelativistic composite fermion theory of Halperin, Lee and Read of the half-filled Landau level.

The rest of the thesis concerns the cuprate high-T_c superconductors ("cuprates"). Conventional wisdom says that beyond the superconducting "dome" in cuprates, the material behaves as a Fermi liquid. However, this picture does not help explain the disappearance of the superconducting order parameter, and there are some anomalous measurements that can-

not be explained by a Fermi liquid phase. It was proposed by Kopp, Ghosal, and Chakravarty that there is a *ferromagnetic* phase at zero temperature beyond the superconducting dome, and that fluctuations of the ferromagnetic order parameter compete with the superconducting order parameter and work to suppress the superconducting transition temperature [KGC07]. In Chapter 3 we summarize the experimental evidence for ferromagnetic fluctuations in the overdoped cuprates, and present several calculations supporting the existence of a ferromagnetic ground state in the 2D single-band Hubbard model, which model is thought to provide an adequate description of the cuprate superconductors.

Another region of interest in the cuprate phase diagram is the pseudogap phase. It is unclear which of a host of competing order parameters is responsible for the behavior in this phase, such as the recent observation of an anomalous thermal Hall conductance in the cuprate $La_{2-x}Sr_xCuO_4$ [GLB19]. One promising candidate is the d-density wave state. In Chapter 4, we investigate the effect that density wave states have on the localized spins of a square lattice. We derive the effective Dzyaloshinskii-Moriya (DM) interaction from first principles and study its effects on both ferromagnetic and antiferromagnetic backgrounds. We find that topologically nontrivial density wave states can induce stable DM interactions among the localized spins of the lattice when an external magnetic field is present. Furthermore, these density wave-induced DM vectors point along the external magnetic field's direction–implying that they break time-reversal and spin rotation symmetries in the same manner. Due to these symmetry considerations alone we find that the underlying magnon excitations cannot induce any thermal Hall effect. Utilizing a Holstein-Primakoff substitution about a mean-field ground state expansion we calculate the topological density wave corrections to magnetic ground state energy, spin canting angles, and the dispersion of the magnons for both the ferromagnetic and antiferromagnetic cases.

The dissertation of Nicholas Demetrios Rombes III is approved.

Stuart Brown

Michael Mulligan

Per Kraus

Sudip Chakravarty, Committee Chair

University of California, Los Angeles

2020

To my parents

who have supported me

from third coast to west,

from near and from afar

TABLE OF CONTENTS

LIST OF FIGURES

VITA

2014	B.S. (Physics) and B.S. (Mathematics), University of Michigan, Ann Arbor.
2016	M.S. (Physics), UCLA, Los Angeles, California.
2014–2020	Teaching Assistant, Department of Physics and Astronomy, UCLA.

PUBLICATIONS AND PRESENTATIONS

Nicholas Rombes and Sudip Chakravarty. "Specific heat and pairing of Dirac composite fermions in the half-filled Landau level." *Annals of Physics*, **409**:167915, October 2019.

Powell, I. E., Durr, S., Rombes, N. and Chakravarty, S. *Density Wave Mediated Dzyaloshinskii Moriya Interactions.* In preparation.

Rombes, N., & Chakravarty, S. *Superconductivity in the half-filled Landau Level.* Bhaumik Luncheon Young Scientists Seminar (2019).

Rombes, N., & Chakravarty, S. *Specific heat and pairing of Dirac composite fermions in the half-filled Landau level.* Gordon Research Conference, Correlated Electron Systems: Entanglement and Coherence in Quantum Materials (2018).

CHAPTER 1

Introduction

Condensed matter physicists in the first half of the twentieth century classified phases of matter using the Landau-Ginzburg paradigm of broken symmetry leading to a local order parameter, which describes phenomena as diverse as the development of magnetism in metals and the formation of ice crystals from water. The discovery of the integer quantum Hall effect (IQHE) by von Klitzing et al. [KDP80] and the fractional quantum Hall effect (FQHE) by Tsui et al. [TSG82] in which systems of electrons subject to a strong magnetic field exhibit wildly different behavior depending on how much of the highest Landau level is filled challenged this paradigm; these systems apparently possess phases which can not be described by such a local order parameter. This prompted the development of the notion of topological order to describe the physics of such systems. A description of the IQHE and FQHE due to Jain emerged using the concept of "composite fermions", in which the combination of an electron with a number of flux quanta are treated as the fundamental degrees of freedom in the system [Jai89]. This description has the beautiful feature that the FQHE of the electrons can be interpreted as the IQHE of the composite fermions, and provides an example in which a strongly-interacting system can be transmuted into a weakly-interacting system with the correct choice of degrees of freedom.

Of particular interest is the state in the quantum Hall system in which one-half of the highest Landau level is filled, due in part to the unexpected observation of a gap [WES87] and to some anomalous transport measurements [WPR90]. States with filling fractions of even denominator are traditionally less well-understood than their odd-denominator counterparts. Halperin, Lee, and Read again used composite fermions to describe this state, mostly to the satisfaction of the theoretical community [HLR93]. However, recently it has been pointed

out by D. T. Son that the traditional composite fermion description propounded by Halperin et al. does not superficially obey the same symmetry as the system it attempts to describe, and a new description in terms of *relativistic* Dirac composite fermions has been offered that does possess the relevant symmetry [Son15]. A natural question is then whether there is any observable difference between these two descriptions. In Chapter 2 we compute the contribution to the specific heat by these Dirac composite fermions at low temperature, and show that it is identical to the specific heat contribution in the non-relativistic picture. We also show that these Dirac composite fermions can pair up into superconducting pairs by numerically solving the coupled Eliashberg equations, in an extension of previous work by Wang and Chakravarty [WC16b].

Another topic of enormous contemporary relevance is the high-T_c superconductors. For almost 80 years the discovery of superconductivity by Onnes in 1911, superconductors were limited to transition temperatures less than 23 K, and are well-described by the microscopic theory propounded by Bardeen, Cooper, and Schrieffer [BCS57]. The discovery [BM89] of materials with superconducting transition temperatures much larger, and in unexpected materials (doped copper oxides, or "cuprates", now with transition temperatures up to 133 K), challenged the traditional BCS picture. The undoped parent compounds of these unconventional superconductors are Mott insulating antiferromagnets, and the problem of exactly how adding charge carriers to such a Mott insulator can produce superconductivity has provided a driving motive in the condensed matter community for decades [LNW06].

A further mystery is how beyond a certain critical doping, the superconducting transition temperature drops and eventually vanishes; see Figure 1.1 for a simplified phase diagram for high-T_c cuprates. Conventional wisdom says that beyond the superconducting "dome", the material behaves as a Fermi liquid. However, this picture does not help explain the disappearance of the superconducting order parameter, and there are some anomalous measurements that cannot be explained by a Fermi liquid phase. It was proposed by Kopp, Ghosal, and Chakravarty that there is a *ferromagnetic* phase at zero temperature beyond the superconducting dome, and that fluctuations of the ferromagnetic order parameter com-

pete with the superconducting order parameter and work to suppress the superconducting transition temperature [KGC07]. In Chapter 3 we summarize the experimental evidence for ferromagnetic fluctuations in the overdoped cuprates, and present several calculations supporting the existence of a ferromagnetic ground state in the 2D single-band Hubbard model, which model is thought to provide an adequate description of the cuprate superconductors.

Another puzzling region of the cuprate phase diagram is the so-called "pseudogap" phase, found to the left of the line marked T^* in Figure 1.1. It is so far unclear which of a variety of order parameters is responsible for the development of the gap in this phase. One candidate is the d-density wave [CLM01]. In Chapter 4 we discuss the relevance of this state to a recent experiment [GLB19] that showed an anomalous thermal Hall conductance in the pseudogap phase of a cuprate superconductor. Recently Zi-Xiang Li and Dung-Hai Lee have shown that the d-density wave produces a nonzero thermal Hall conductance [LL19], and Samajdar, Scheurer et al. have shown that there can be spin-wave contributions to the thermal Hall effect [SCS19]. With these results in mind, we investigate the effects that a d-density wave can have on an underlying spin system (both ferromagnetic and antiferromagnetic), and show that it produces an effective Dzyaloshinskii-Moriya interaction. We show that the excitations of the resulting effective magnetic Hamiltonian *can not* contribute to the thermal Hall effect. However, the signatures of the d-density wave on the underlying spin system could be used to detect the presence of such a state and thus assess its relevance to the pseudogap phase of the cuprates.

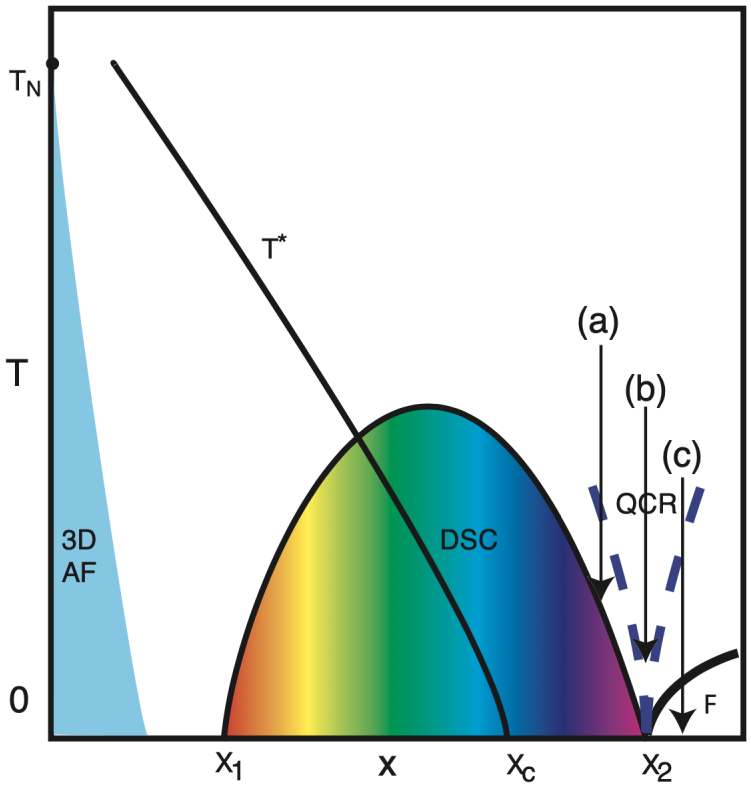

Figure 1.1: Simplified phase diagram of the cuprate superconductors. x is hole doping. Near $x = 0$ is the Mott insulating antiferromagnetic phase. In rainbow is the superconducting "dome" bounded by the superconducting T_c, which terminates at critical points x_1 and x_2 in the underdoped and overdoped regimes, respectively. T^* marks the (rightmost) boundary of the pseudogap phase, which presumably terminates in a critical point x_c obscured by the superconducting dome. It is conjectured in [KGC07] that x_2 separates the superconducting phase from a ferromagnetic phase, and that competition between the superconducting and ferromagnetic order parameters is responsible for the decline in T_c near x_2. (a), (b), and (c) represent possible experimental trajectories, and there should be a quantum critical fan above the critical point x_2. Reproduced from [KGC07] with permission.

CHAPTER 2

The Half-Filled Landau Level

Portions of this chapter are adapted from the publication:

Nicholas Rombes and Sudip Chakravarty. "Specific heat and pairing of Dirac composite fermions in the half-filled Landau level." *Annals of Physics*, **409**:167915, October 2019.

2.1 Introduction

2.1.1 Integer quantum Hall effect

Classically, the application of a uniform magnetic field to a system of electrons leads to cyclotron motion, and the allowed kinetic energy of the electrons is continuous. Quantum mechanically, the electrons in their cyclotron motion are "bound", and one expects quantization of energy levels, which is borne out by the diagonalization of the single-electron Hamiltonian

$$H = \frac{(\mathbf{p} - e\mathbf{A})^2}{2m}. \tag{2.1}$$

One finds that the allowed energy levels are evenly spaced, macroscopically degenerate *Landau levels* (LLs), $E_n = (n + 1/2)\hbar\omega_c$, whose spacing and degeneracy grow linearly with the magnetic field. If one considers a macroscopic sample and ignores Coulomb interactions between electrons, the picture is that of a Fermi sea of filled LLs, the total fraction of Landau levels filled denoted ν; disorder in a system broadens the LLs some width that is typically less than the LL separation (see Figure 2.1). It is clear from this simple picture that as we

tune the magnetic field, we will find two distinct behaviors, depending on whether the Fermi energy lies within one of the LLs ($\nu \notin \mathbb{Z}$) or in the region with vanishingly low density of states between the LLs ($\nu \in \mathbb{Z}$).

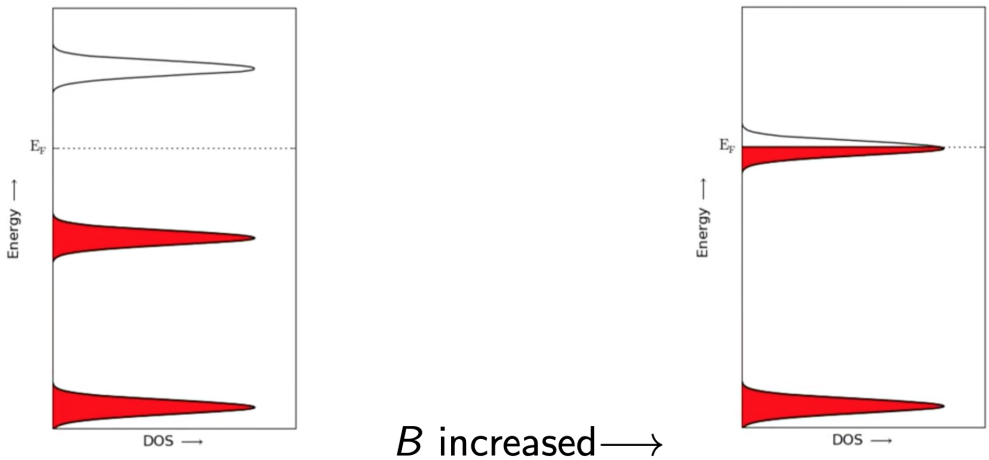

Figure 2.1: Cartoon of the effect of tuning the magnetic field in the quantum Hall system. On the left, the Fermi level lies in between Landau levels, in a region of zero density of states. This state is gapped. On the right, the Fermi level lies within a disorder-broadened Landau level. This state is gapless.

The quantum-mechanical behavior is essentially two-dimensional, since the electrons are free along the direction of the applied field. Indeed, when one measures the transport properties of a two-dimensional electron gas (2DEG) one finds distinct plateaux at *quantized* values of the Hall resistivity [KDP80] (see Figure 2.2):

$$\rho_{xy} = \frac{h}{e^2}\frac{1}{\nu}, \qquad \nu \in \mathbb{Z}. \tag{2.2}$$

This is known as the *integer quantum Hall effect* (IQHE), and can be understood without reference to the electronic Coulomb interaction. The key feature is that a gap opens up at particular values of the magnetic field due to LL quantization.

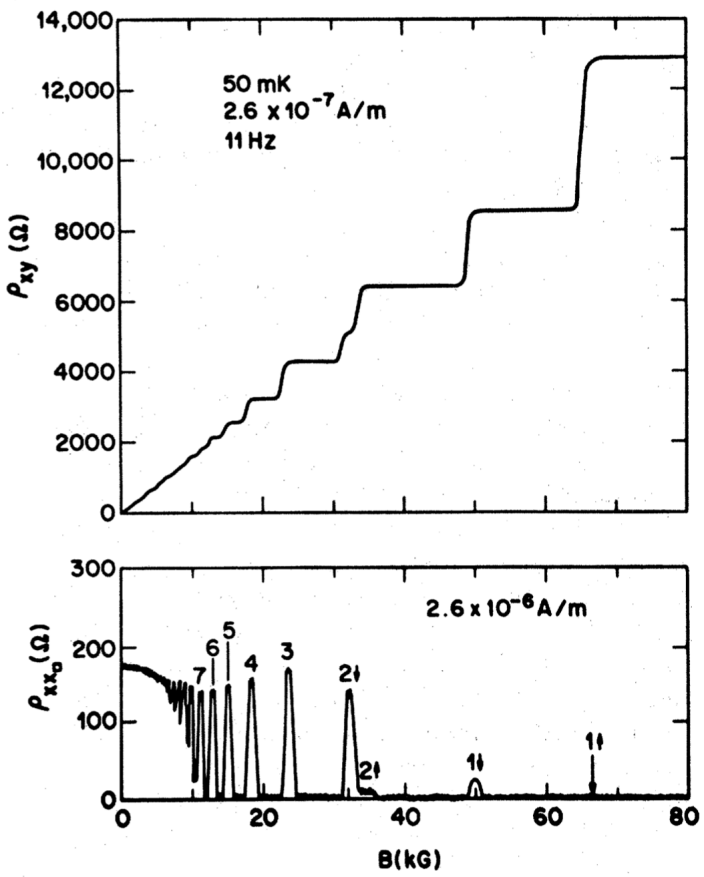

Figure 2.2: The integer quantum Hall effect. Hall (top) and diagonal (bottom) resistivity as a function of magnetic field. At large magnetic fields, the peaks for spin-up and spin-down electrons are resolved. Reproduced from [PTG82].

2.1.2 Fractional quantum Hall effect

As advances in experimental and fabrication techniques allowed for higher-mobility samples and larger magnetic fields, the condensed matter community was met with a surprise: there were plateaux found at *fractional* filling of a Landau level [TSG82]. It was established that plateaux emerge at filling fractions

$$\nu = \frac{p}{2pq \pm 1}, \qquad p, q \in \mathbb{Z}, \tag{2.3}$$

the strongest of which occur at $q = 1$. It is clear that this new fractional quantum Hall effect (FQHE) cannot be explained using a non-interacting picture, since the non-interacting

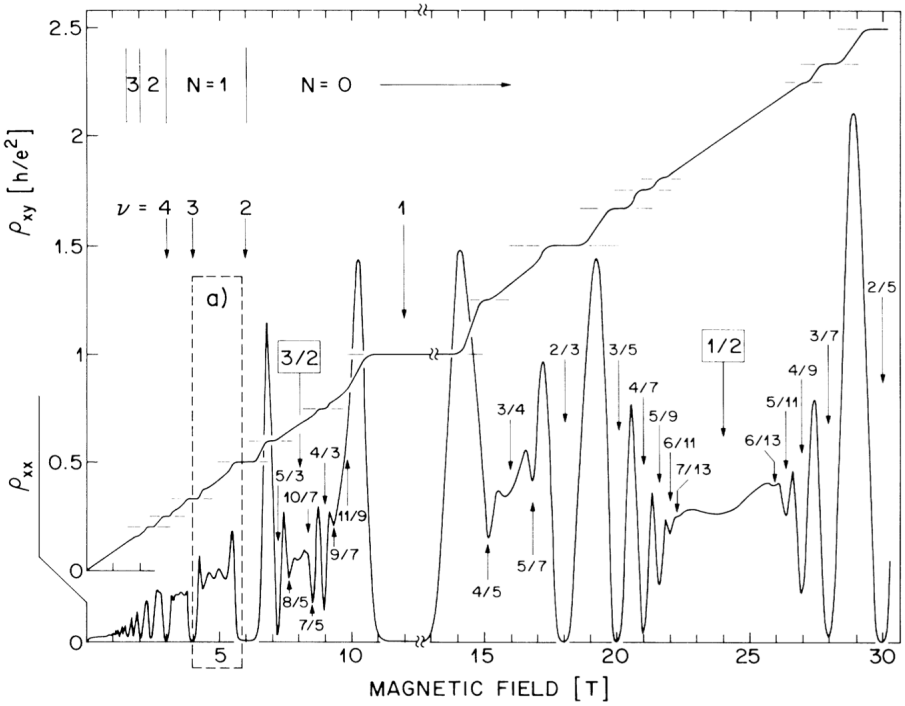

Figure 2.3: The fractional quantum Hall effect. Hall and diagonal resistivity as a function of magnetic field. The high-field diagonal resistivity amplitude is reduced by a factor of 2.5 for clarity. Reproduced from [WES87].

picture is essentially exactly solved. Why does a gap open up at these non-integer filling fractions? A flurry of theoretical work followed, attempting to gain some traction on the problem of a 2DEG with Coulomb interaction included:

$$H = \sum_i \frac{(\mathbf{p}_i - e\mathbf{A})^2}{2m} + \frac{1}{2}\sum_{i \neq j} \frac{e^2}{|\mathbf{r}_i - \mathbf{r}_j|}. \tag{2.4}$$

Laughlin [Lau83] wrote down a trial wave function for the "extreme quantum" limit where all of the electrons lie in the lowest LL, for the special cases of filling fractions $\nu = 1/m$ for odd m:

$$\psi_{1/m}(z_i) = \prod_{j<i} (z_j - z_i)^m e^{-\frac{1}{4}\sum_l |z_l|^2}, \tag{2.5}$$

where $z_i = x_i + iy_i$ are the electron coordinates. This wave function compares favorably with the exact ground state for a small number of particles, and has many interesting features, most notably that quasiparticle excitations above this ground state carry *fractional charge*

$e^* = e/m$ and have *fractional statistics*, where an exchange of two quasiparticles gives a phase of $e^{2\pi i/m}$. It is clear that this wave function can only describe odd-denominator filling fractions, in order to maintain the overall fermionic character of the many-electron wave function.

How, then, do we explain the filling fractions $p/(2p+1)$ for $p \neq 1$? A hint comes if one notices that if the magnetic field strength is such that the filling fraction is $\nu = \frac{1}{m}$, then the number of magnetic flux quanta is m times the number of electrons in the system; in particular, the lowest LL being completely filled corresponds to having one magnetic flux quantum per electron. It is here that the fundamentally two-dimensional nature of this problem emerges: in two dimensions with a perpendicular magnetic field, one can "attach" some number of magnetic flux quanta to the bare electrons, to form so-called *composite fermions* (CFs) [Jai89]. For each magnetic flux quantum attached, upon exchange of the locations of the composite fermions, the wave function receives a factor of -1 (the Aharonov-Bohm effect), and so if we attach an even number of flux quanta, we are left with fermions again, which feel an effectively reduced magnetic field. This provides an intuitive explanation for the FQHE at filling fractions $1/m$ for odd m; if there are m flux quanta per electron, and we attach $m-1$ flux quanta to each electron to form CFs, then there is one flux quantum left per composite fermion, which corresponds to an entirely filled LLL. The FQHE can be interpreted as the IQHE for CFs! One has traded a problem of interacting electrons for a problem of noninteracting CFs, which are to be interpreted as the true particles of the system.

2.1.3 The half-filled Landau level

The above picture ends up providing a good explanation for odd-denominator filling fractions. However, later experimental developments yielded yet another surprise: a plateau at $\nu = 5/2$ [WES87], and the absence of a plateau in the Hall resistivity but a dip in the diagonal resistivity at $\nu = 1/2$ [JSI89]. Additional experiments at these filling fractions detected an enhanced effective mass of whatever quasiparticle this state supports [DST94] and

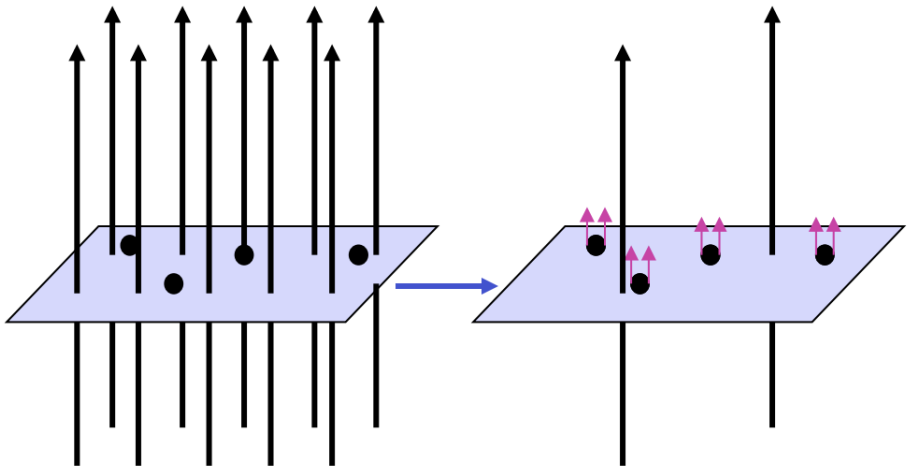

Figure 2.4: Composite fermions imagined as fluxes attached to electrons. Reproduced from `http://www.personal.psu.edu/jkj2/Buckley_Prize_Talk.pdf`.

anomalous acoustic wave propagation [WPR90]. A FQHE state here resists explanation by either Laughlin's wave function or the IQHE of CFs. These observations lead us to attempt to consider $\nu = 1/2$ as a gapless parent state from which the gapped $\nu = 5/2$ state descends. Can we continue to use the composite fermion idea to understand the state at half-filling? At $\nu = 1/2$, when two flux quanta are attached to the bare electrons, the resulting CFs see on average a *zero* magnetic field. This suggests the possibility that the CFs can form a well-defined Fermi surface, and that one can use conventional Fermi-liquid theory to understand the state. This was accomplished by Halperin, Lee, and Read, in the development of what is now known as HLR theory [HLR93].

The mathematical tool that implements flux attachment is the addition of a dynamical Chern-Simons (CS) gauge field a_μ to the action of the electrons:

$$\mathcal{L} = \frac{e\pi}{2\theta\phi_0}\epsilon^{\mu\nu\rho}a_\mu\partial_\nu a_\rho - \frac{1}{2m}\psi^\dagger[-i\nabla - e\mathbf{A} - e\mathbf{a}]^2\psi, \tag{2.6}$$

where e and m are the electron charge and mass, θ is related to the Chern-Simons level, ϕ_0 is the flux unit, and $\mathbf{A}$ is the physical external magnetic potential. Here Roman indices take values 1,2,3, and boldface symbols indicate vectors with zero transverse component. The CS term is only gauge invariant in two dimensions, this mathematical fact reflecting the

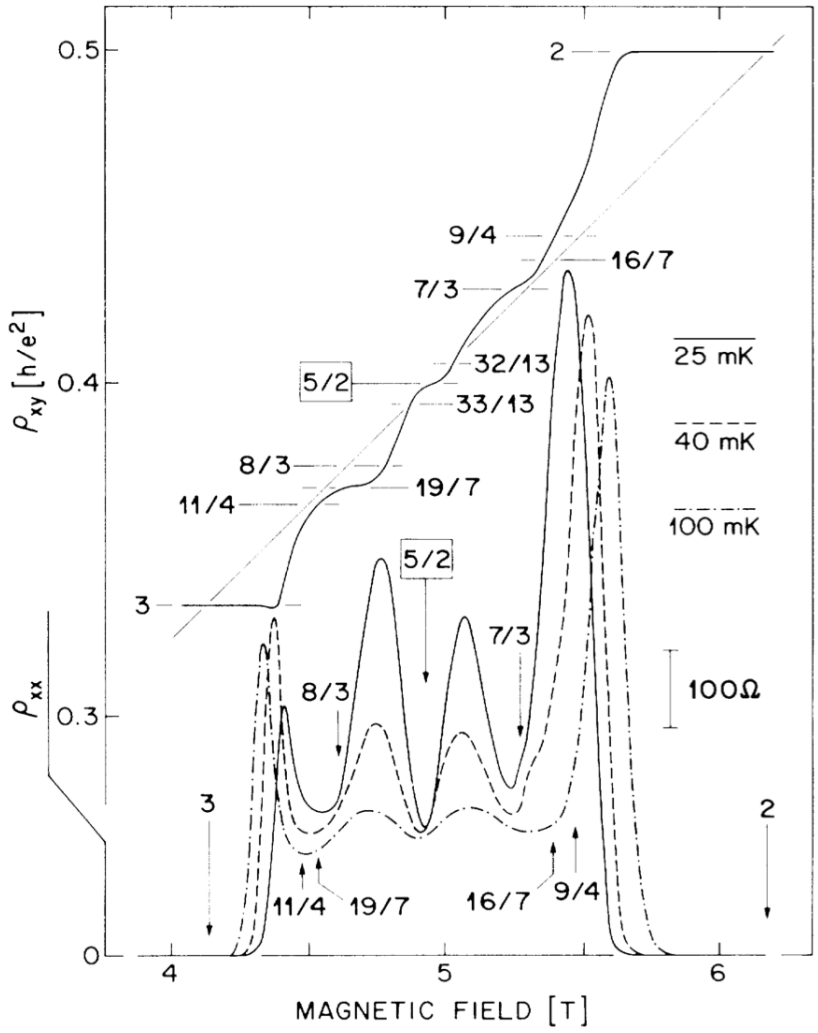

Figure 2.5: Hall and diagonal resistivity as a function of magnetic field. Development of a plateau at $\nu = 5/2$. Reproduced from [WES87].

reality of the two-dimensional nature of flux attachment. This is an *exact* procedure, and so the question becomes how fluctuations of the CS gauge field affect the mean-field Fermi surface of CFs. HLR theory shows that these fluctuations tend to enhance the effective mass of the CFs and can explain the observed anomalous acoustic wave propagation, but do not necessarily destroy the Fermi surface, and so the picture of $\nu = 1/2$ as a Fermi sea of CFs seems solid. HLR theory is thus treated as a launching pad from which to understand any states descending from $\nu = 1/2$. Beginning from HLR theory, one can look for instabilities in the $\nu = 1/2$ state towards ordered states due to fluctuations in the gauge field, which could

give rise to the gap seen at $\nu = 5/2$. One idea is that the CFs pair up into superconducting Cooper pairs. It was found that the Fermi surface of CFs is always unstable at the mean-field level towards Cooper pairs in odd angular momentum channels [GWW92]. A refinement of this work using random-phase approximation (RPA) corrections found that fluctuations of the CS gauge field lead to a current-current interaction between the CFs that is repulsive in the limit of small Matsubara frequencies, and which dominate over other interactions when the gap is small [Bon99]. This seems to rule out the idea of a continuous phase transition between the HLR state and a paired state. However, an extension of this analysis to the entire Matsubara frequency range revealed that the current-current interaction may be attractive at higher Mastubara frequencies for angular momentum channels $\ell \geq 2$, salvaging the possibility of such a continuous phase transition [WMC14].

2.1.4 Particle-hole symmetry

It was pointed out [Son15] that a half-filled lowest LL possesses an approximate symmetry that cannot be made sense of in HLR theory. In a very large magnetic field the LLs can be thought of as practically infinitely separated, and all the physics is contained in the interactions of the electrons in just the lowest LL. In this truncated Hilbert space, one can equally well describe $\nu = 1/2$ as an empty LL half-populated with electrons, or a *full* LL half-depleted with holes: there is particle-hole (PH) symmetry in this limit. Thus one expects a correct description of this state to reflect this PH symmetry. However, HLR theory makes no reference to the unpopulated states above half-filling, and explicitly attaches flux to electrons: there is no obvious way to make the PH symmetry apparent. Indeed, the CS term in the effective action, which implements the flux attachment, seems to spoil this symmetry in HLR theory. Thus, recently, a radical description of the half-filled Landau level was proposed, in which the CFs are now massless Dirac particles, and there is no CS term for the emergent gauge field [Son15]. In this theory, PH symmetry is explicitly incorporated at half filling. It is a matter of debate whether these two descriptions, the HLR description and the Dirac CF description, represent equivalent formulations of the half-filled Landau

level, and whether there are experiments that are consistent with the Dirac formulation but inconsistent with HLR theory [GZM16, LS17, WCH17, PKB17, KMR19, KRM19].

In this work we participate in this debate. Firstly, we construct a pairing mechanism for the Dirac CFs, and show that pairing is possible (with minor differences from previous work from our group [WC16b]) in angular momentum channels apart from $\ell = 0$, for which we do not find pairing to be possible. Secondly, we compute the low-temperature specific heat of the Dirac CFs, which *does not* differ from the corresponding result in HLR theory. The present Eliashberg calculation involves solving both the coupled equations involving the order parameter and the Eliashberg-Z factor. We furthermore make use of the Luttinger formula for the free energy [Lut60]. It was shown [CS98] that this expansion fails in general for interacting fermionic systems in 2D; however, it is valid here in at least the leading order because the vertex correction vanishes, as shown from the Ward identity in Section 2.5.2. Thus the present approximation is on much firmer footing than in [WC16b]. The following chapter is an adapted version of [RC19].

2.2 Model

The low-energy effective action for the Dirac CF is given by [Son15]

$$S_{\text{CF}} = \int d^3x \{ i\overline{\psi}\gamma_\mu(\partial_\mu + ia_\mu)\psi + \frac{1}{4\pi}\epsilon^{\mu\nu\lambda}A_\mu\partial_\nu a_\lambda \}, \tag{2.7}$$

where $\{\gamma_0, \gamma_1, \gamma_2\} = \{\sigma_3, \sigma_1, \sigma_2\}$ are the Pauli matrices, $\overline{\psi} = \psi^\dagger\gamma_0$, and we have set $\hbar = v_F = 1$. In this work, Greek indices run from 0 to 2 and Roman indices run from 1 to 2. Compare this to Equation (2.6): this action is missing the CS term for a_μ, in place of the background field term Ada, and involves Dirac fermion operators instead of nonrelativistic fermion operators. This action describes massless, electrically neutral Dirac fermions that are charged under an emergent gauge field a_μ. How are these Dirac fermions related to the physical external magnetic field and physical electrons? Differentiating Equation (2.7) with respect to a_0, we see that

$$\overline{\psi}\gamma_0\psi = \frac{\nabla \times \mathbf{A}}{4\pi}. \tag{2.8}$$

The density of Dirac CFs is set by the physical external magnetic field, and is *not* the same as the density of physical electrons, in contrast to the HLR description. Differentiating with respect to A_0, we find

$$\rho_e' = \frac{\nabla \times \mathbf{a}}{4\pi}. \tag{2.9}$$

Since the emergent gauge field strength $b \equiv \nabla \times \mathbf{a}$ should be zero at half-filling, we interpret ρ_e' as the difference between the physical electron density and its value at half-filling: $\rho_e' = \rho_e - \rho_{\nu=1/2}$. Thus the strength of the emergent gauge field is set by the physical electron density. The gauge field mediates an interaction between the Dirac CFs, which we show in detail in the following section.

2.2.1 Effective interaction

This section follows [WC16b] closely. In order to investigate possible pairing of Dirac CFs mediated by the exchange of the gauge bosons, we must write down a kinetic term for the emergent gauge field. There are two possible terms: a Maxwell term, $S_{\text{Max}} \sim F_{\mu\nu}F^{\mu\nu}$, with $F_{\mu\nu} \equiv \partial_\mu a_\nu - \partial_\nu a_\mu$, and a term induced by the Coulomb interaction between the *physical* electrons (see Equation (2.9))

$$S_C \sim \frac{e^2}{\epsilon_r} \int d\mathbf{x}_1 d\mathbf{x}_2 \frac{\rho_e'(\mathbf{x}_1)\rho_e'(\mathbf{x}_2)}{|\mathbf{x}_1 - \mathbf{x}_2|} \tag{2.10}$$

where ϵ_r is the dielectric constant of the background material. In momentum space, we see that $S_{\text{Max}} \sim |\mathbf{k}|^2$ and $S_C \sim \mathbf{k}$; thus the low-energy dynamics will be dominated by the Coulomb term, and that is the term we will keep.

Using the Coulomb gauge, the momentum-space Coulomb action becomes

$$S_C = \frac{1}{2}\frac{e^2}{8\pi\epsilon_r} \int \frac{d\Omega d^2\mathbf{k}}{(2\pi)^3} a_T(k)|\mathbf{k}|a_T(-k), \tag{2.11}$$

where we have Wick rotated so that Ω are zero-temperature Matsubara frequencies, $k \equiv (i\Omega, \mathbf{k})$, and $a_T(\mathbf{k}) \equiv \epsilon_{ij}\hat{k}_i a_j(\mathbf{k})$ is the transverse component of the gauge field. We see that the bare transverse gauge field propagator takes the form

$$D_T^{(0)}(k) = \frac{8\pi\epsilon_r}{e^2}\frac{1}{|\mathbf{k}|}. \tag{2.12}$$

We can now integrate out the transverse gauge field to obtain a current-current interaction:

$$S_{\text{int}} = \frac{1}{2}\int \frac{d\Omega d^2\mathbf{k}}{(2\pi)^3} J_T(k) D_T^{(0)}(k) J_T(-k), \tag{2.13}$$

with the transverse CF current operator given by $J_T(k) = \epsilon_{ij}\hat{k}_i\, i\int \frac{d\omega d^2\mathbf{q}}{(2\pi)^3}\overline{\psi}(q+k)\gamma_i\psi(q)$. Since Equation (2.7) is a low-energy effective action, it will be valid only near the Fermi surface, and so we must project this interaction to the Fermi surface. To achieve this, we make the replacement [KMT15]

$$\psi(k) \to P_{\mathbf{k}}^{(+)}\psi(k) = \frac{1}{\sqrt{2}}\begin{pmatrix} ie^{-\theta_{\mathbf{k}}} \\ 1 \end{pmatrix}\chi(k), \tag{2.14}$$

where $P_{\mathbf{k}}^{(+)} \equiv \frac{1}{2}(1 + i\gamma_0\vec{\gamma}\cdot\hat{k})$ is the projection operator onto the positive energy branch of the Dirac CF. This gives us an interaction between scalar fields $\chi(k)$,

$$S_{\text{int}} = \frac{1}{2}\int\prod_{i=1}^{4}\frac{d\omega_i d^2\mathbf{k}_i}{(2\pi)^3}(2\pi)^3\delta^{(3)}(k_3+k_4-k_2-k_1)\frac{8\pi\epsilon_r}{e^2}\frac{e^{-\frac{i}{2}[\theta_{\mathbf{k}_1}+\theta_{\mathbf{k}_2}-\theta_{\mathbf{k}_3}-\theta_{\mathbf{k}_4}]}}{|\mathbf{k}_3-\mathbf{k}_1|}\chi^\dagger(k_4)\chi^\dagger(k_2)\chi(k_3)\chi(k_1). \tag{2.15}$$

We now consider the contribution to the action from the BCS channel, $k_1 = -k_2 \equiv k \equiv (\omega, \mathbf{k})$ and $k_3 = -k_4 \equiv k' \equiv (\omega', \mathbf{k}')$, near the Fermi surface, $|\mathbf{k}| = |\mathbf{k}'| \approx k_F$:

$$S_{\text{BCS}} = \int \frac{d\omega d\theta_{\mathbf{k}}}{(2\pi)^2}\frac{d\omega' d\theta_{\mathbf{k}'}}{(2\pi)^2}\frac{4\pi\epsilon_r}{k_F e^2}\frac{e^{-i[\theta_{\mathbf{k}}-\theta_{\mathbf{k}'}]}}{|\sin\frac{\theta_{\mathbf{k}}-\theta_{\mathbf{k}'}}{2}|}\chi^\dagger(-k')\chi^\dagger(-k)\chi(k')\chi(k). \tag{2.16}$$

From here on, we set $k_F = 1$. From here we can read off an effective BCS-channel (or particle-particle) interaction

$$V_{\text{BCS}}(\mathbf{k},\mathbf{k}') = 2\alpha\frac{e^{-i[\theta_{\mathbf{k}}-\theta_{\mathbf{k}'}]}}{|\sin\frac{\theta_{\mathbf{k}}-\theta_{\mathbf{k}'}}{2}|}, \tag{2.17}$$

where we have introduced an effective coupling constant for Dirac CFs $\alpha \equiv \epsilon_r/e^2$. It is clear that this potential is repulsive in all angular momentum channels, and with this bare interaction, no pairing is possible. In order to generate an attractive interaction, we introduce an RPA-corrected potential, with a correction from screening due to the finite density of Dirac CFs:

$$V_{\text{BCS,RPA}}(k,k') = 2\alpha\frac{e^{-i[\theta_{\mathbf{k}}-\theta_{\mathbf{k}'}]}}{|\sin\frac{\theta_{\mathbf{k}}-\theta_{\mathbf{k}'}}{2}| + \alpha|\omega-\omega'|}. \tag{2.18}$$

Breaking this up into angular momentum channels, we generate an effective interaction

$$V_{\ell'}(i\Omega) \equiv \alpha \int \frac{d\theta}{2\pi} \frac{e^{i(\ell'-1)\theta}}{|\sin\frac{\theta}{2}|} \frac{2}{1+\alpha\frac{|\Omega|}{|\sin\frac{\theta}{2}|}}. \tag{2.19}$$

where $\Omega \equiv \omega' - \omega$ and $\omega \equiv \theta_{\mathbf{k}} - \theta_{\mathbf{k}'}$. This ℓ' is the angular momentum channel for the scalar field $\chi(k)$; its relationship to ℓ, the angular momentum channel of the Dirac CF, depends on the nature of the order parameter $\hat{\Delta}(k) \equiv [\Delta_s(k) + \mathbf{d}(k)\cdot\boldsymbol{\sigma}]i\sigma_2$. For the pseudospin singlet order parameter, $\hat{\Delta}(k) = \langle\psi^T(-k)P^{(+)}_{-\mathbf{k}}i\sigma_2 P^{(+)}_{\mathbf{k}}\psi(k)\rangle$, $\ell = \ell' - 1$, and in order to satisfy antisymmetry of $\hat{\Delta}(k)$, ℓ must be even. For the pseudospin triplet, $\hat{\Delta}(k) = \langle\psi^T(-k)P^{(+)}_{-\mathbf{k}}(\mathbf{d}\cdot\boldsymbol{\sigma})(i\sigma_2)P^{(+)}_{\mathbf{k}}\psi(k)\rangle$, ℓ must be odd, and either $\ell = \ell'$ or $\ell = \ell' - 2$, depending on which triplet state the pair is in.

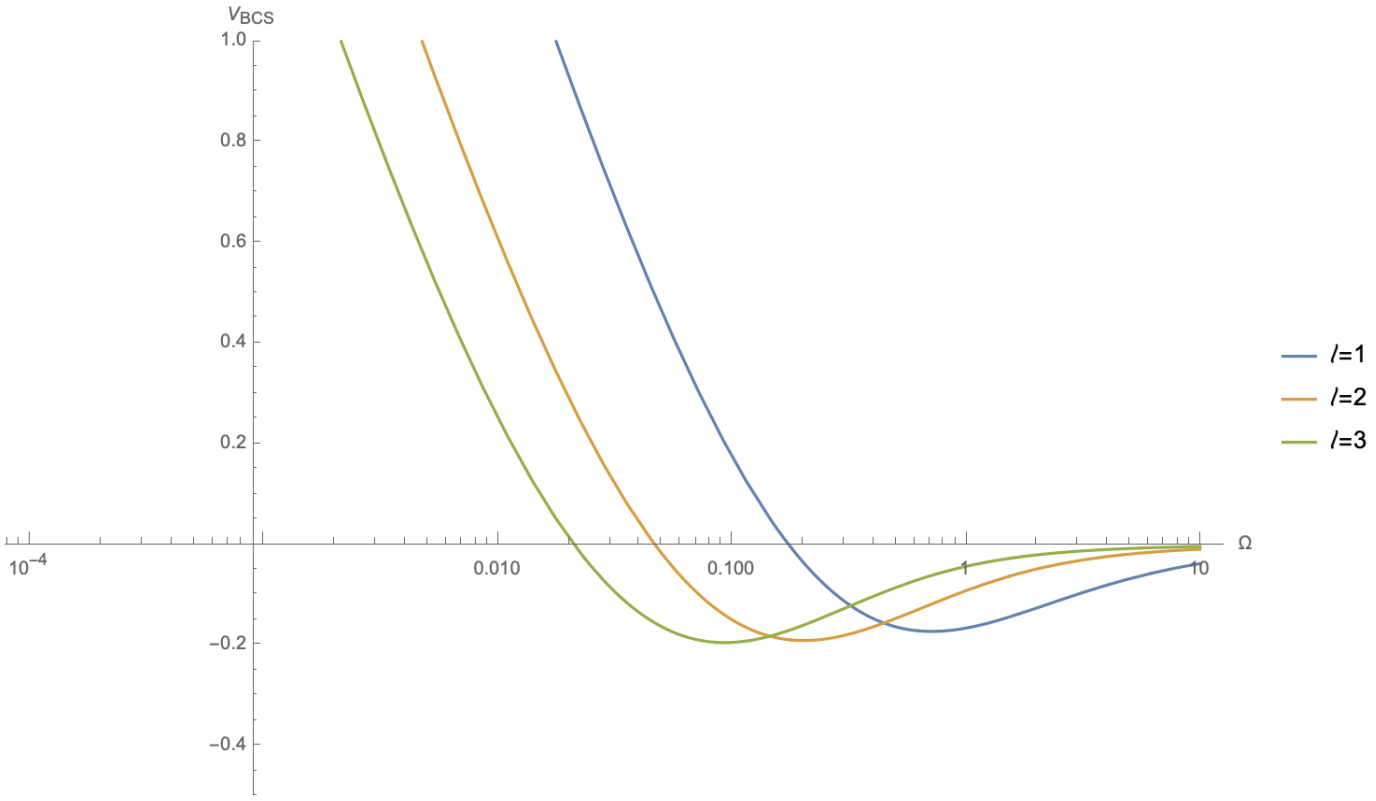

Figure 2.6: Potential felt between Dirac CFs as a function of Matsubara frequency, measured in units of ϵ_F, for angular momentum channels $\ell = 1, 2, 3$.

2.2.2 Eliashberg equations

We are interested in whether this potential leads to pairing; we can look then at how the exchange of this gauge boson affects the fermion propagator. Pairing will show up as off-diagonal contributions to the Dirac fermion propagator, which are simply the expectation values $\langle\psi^+\psi^+\rangle$, where $\overline{\psi}^\dagger = ((\psi^+)^\dagger, (\psi^-)^\dagger)$ is the Dirac fermion containing particles ψ^+ and antiparticles ψ^-. The full propagator of the Dirac fermions is

$$G^{-1}(\mathbf{p}, i\omega_n) = G_0^{-1}(\mathbf{p}, i\omega_n) - \Sigma(\mathbf{p}, i\omega_n), \tag{2.20}$$

where G^0 is the free fermion propagator and Σ is the fermion self-energy, which we parametrize in the standard way as

$$\Sigma(\mathbf{p}, \omega_n) = \begin{pmatrix} [1 - Z(\mathbf{p}, \omega_n)]i\omega_n + \chi(\mathbf{p}, \omega_n) & \phi(\mathbf{p}, \omega_n) \\ \phi^*(\mathbf{p}, \omega_n) & [1 - Z(\mathbf{p}, \omega_n)]i\omega_n - \chi(\mathbf{p}, \omega_n) \end{pmatrix}, \tag{2.21}$$

where Z is the mass renormalization, χ is a kinetic energy renormalization, and ϕ is the anomalous self-energy. This propagator describes the dynamics of both particles and antiparticles contained in $\overline{\psi}$, hence the 2×2 matrix. Exchange of the gauge field a_μ, which leads to the effective interaction Equation (2.19), will produce corrections to Σ. In particular, if the potential leads to pairing, the fermions will pick up a contribution to ϕ.

Calculation of Σ amounts to calculating an infinite number of loop diagrams. However, if one neglects any diagram containing a loop correction to the fermion-gauge field vertex, one is left summing "rainbow diagrams" and can write down the self-consistent Dyson equation

$$\Sigma^{\alpha\beta}(\mathbf{p}, i\omega) = \frac{1}{\beta}\sum_m \int \frac{d^3k}{(2\pi)^3} V_{\text{eff}}^{\alpha\gamma}(\mathbf{k}, i\nu; \mathbf{p}, i\omega) G^{\gamma\beta}(\mathbf{k}, i\nu), \tag{2.22}$$

where $V_{\text{eff}}^{\alpha\beta}$ is the effective interaction mediated by the gauge bosons (off-diagonal elements are particle-particle interactions, diagonal elements are particle-hole interactions). This equation is standard in treatments of strong-coupling superconductivity; there, Migdal showed that vertex corrections are small ($\sim \sqrt{m/M}$, where m is the electron mass and M is the ion mass), but for this case there is no such ratios of small parameters. Therefore we must

justify its use by investigating corrections to the Dirac CF-gauge boson vertex. We show that vertex corrections are negligible in Section 2.5.2, and take it for granted moving forward.

Equation (2.19) serves as the kernel in Equation (2.22) after evaluating it on the Fermi surface. We neglect χ as an unimportant kinetic energy term, and we assume that Z has weak momentum dependence, $Z(\mathbf{k}, i\omega) \approx Z(i\omega)$. We can then perform the integral over $\mathbf{k}$, break the equation up into angular momentum channels, and obtain the zero-temperature, imaginary axis Eliashberg equations:

$$\phi_{\ell'}(i\omega) = -\int_{-\infty}^{\infty} \frac{d\nu}{2\pi} V_{\ell'}(i\omega - i\nu) \frac{\phi_{\ell'}(i\nu)}{\sqrt{(\nu Z(i\nu))^2 + |\phi_{\ell'}(i\nu)|^2}} \tag{2.23}$$

$$[1 - Z(i\omega)]\omega = \int_{-\infty}^{\infty} \frac{d\nu}{2\pi} V_{\ell'=1}(i\omega - i\nu) \frac{\nu Z(i\nu)}{\sqrt{(\nu Z(i\nu))^2 + |\phi_{\ell'}(i\nu)|^2}}. \tag{2.24}$$

Our goal will be to numerically solve these coupled integral equations. We will interpret $\Delta_\ell(0) \equiv \phi_\ell(0)/Z(0)$ as the physical superconducting gap.

2.3 Results

2.3.1 Eliashberg Equations

Here we present our numerical results: the solutions to Equations (2.23) and (2.24). The difficulty is that $V_{\ell'}(i\Omega)$ diverges at small Ω, which leads to a divergence of $Z(i\omega)$. To deal with this numerically, we self-consistently introduce a cutoff at the scale of the putative physical gap, $\Delta_{\ell'}(0)$. This regularizes $Z(i\omega)$ and allows the coupled equations to be numerically solved.

It is clear from Figure 2.7 that a finite value of $\Delta_\ell(0)$ is attained for large enough coupling, for $\ell' \geq 2$. For $\ell' = 1$, which corresponds to pairing of Dirac CFs in the $\ell = 0$ mode, the potential is repulsive at all Matsubara frequencies, and thus pairing in this channel is not possible with our pairing mechanism. The results are very similar to those in [WC16b]. On comparison to their numerical work in which $Z \equiv 1$, the enhancement of Z near the critical point leads to an enhancement of the critical coupling. This enhancement is most

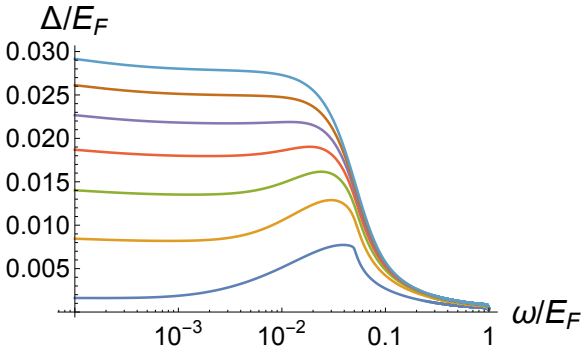

Figure 2.7: Gap vs Matsubara frequency for $\ell' = 2$. From top to bottom: $\alpha = 20, 18, 16, 14, 12, 10, 8$

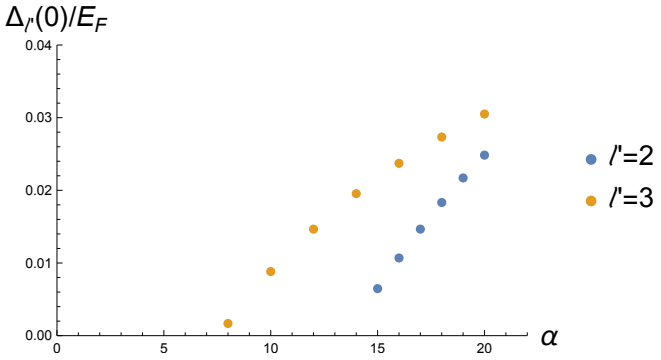

Figure 2.8: Physical gap vs coupling constant for $\ell' = 2, 3$ pairing channels.

pronounced for the $\ell' = 2$ channel, with minimal enhancement for $\ell' > 2$. An inspection of the gap equation reveals that $Z > 1$ tends to suppress the value of the gap at a given coupling, which is consistent with an enhancement of the critical coupling. As long as Z remains finite, which is achieved by a self-consistent cutoff of the potential, the gap will not necessarily collapse to zero for all α, and pairing is possible. The $T = 0$ superconducting transitions appear as quantum critical points.

2.3.2 Specific Heat

We would now like to compute the low-temperature specific heat for the Dirac CFs, including the effects of current-current interactions mediated by the exchange of transverse bosons. To do this, we follow the procedure of [HNP73] and use the formula of Luttinger [Lut60] con-

necting the thermodynamic potential at low temperature to the diagrammatically accessible fermion propagator:

$$\Omega(T) = -V\mathrm{Tr}_s \int \frac{d^2\mathbf{p}}{(2\pi)^2}\frac{1}{2\pi i}\int_{-\infty}^{\infty} dx\{\ln[G^{-1}(p,x-i\epsilon)] - \text{c.c.}\}\frac{1}{e^{\beta(x-\mu)}+1}, \tag{2.25}$$

where the Tr_s traces over the pseudospin degrees of freedom, and V is the system volume. The bare fermion propagator is given by

$$[G^{-1}]^{(0)}(p,i\omega) = i\vec{\gamma}\cdot\mathbf{p} + (i\omega+\mu)\gamma_0, \tag{2.26}$$

and the full propagator, including the fermion self-energy, can be written as

$$G^{-1}(p,i\omega) = i\vec{\gamma}\cdot\hat{p}(|\mathbf{p}| + \Sigma'(p,i\omega)) + (i\omega+\mu+\Sigma''(p,i\omega))\gamma_0. \tag{2.27}$$

It will be convenient to integrate by parts in p, and, differentiating with respect to T to obtain the specific heat, we find

$$c(T) = \frac{1}{8\pi^3 i}\mathrm{Tr}_s\int_0^{2\pi} d\theta\int_0^{\infty} p^2dp\int_{-\infty}^{\infty} dy\{G(p,\mu+yT-i\epsilon)\frac{\partial G^{-1}(p,\mu+yT-i\epsilon)}{\partial p} - \text{c.c.}\}\frac{y^2e^y}{(e^y+1)^2}. \tag{2.28}$$

It will happen that in the region we are interested in, $\Sigma'(p,i\omega) = -\Sigma''(p,i\omega) \equiv \Sigma(p,i\omega)$. Then we can perform the angular integration and the pseudospin trace, and drop a term corresponding to degrees of freedom in the negative-energy band, to find

$$c(T) = \frac{1}{8\pi^2 i}\int_{-\infty}^{\infty} dy\frac{ye^y}{(e^y+1)^2}\int_0^{\infty} dp\,p^2\left\{\frac{1+2\frac{\partial\Sigma(p,\mu+yT-i\epsilon)}{\partial p}}{p+2\Sigma(p,\mu+yT-i\epsilon)-yT+i\epsilon} - \text{c.c.}\right\}. \tag{2.29}$$

The integral over p can be written as a contour integral:

$$\int_0^{\infty} p^2dp\,(\cdots) = \int \overline{p}^2(z)\left(\frac{dz}{z} - \frac{d\overline{z}}{\overline{z}}\right), \tag{2.30}$$

where $z \equiv p + 2\Sigma(p,\mu+yT-i\epsilon) - yT$, and $\overline{p}(z)$ is the solution of $[p+2\Sigma(p,\mu+yT-i\epsilon)-yT]_{p=\overline{p}(z)} = z$. The contour of integration is that for which $\overline{p}(z)$ is real. Along this contour, $\mathrm{Im}\,z = 2\mathrm{Im}\,\Sigma(p,\mu+yT-i\epsilon)$. In general, this is of order $\mathcal{O}(T^2)$; however, we show that near $z=0$, the behavior is instead of $\mathcal{O}(T)$. Thus as $T\to 0$, we can approximate $\overline{p}^2(z) = \overline{p}^2(\overline{z}) - 4i\overline{p}(\overline{z})\mathrm{Im}\,(\overline{z})\frac{d\overline{p}(\overline{z})}{d\overline{z}}$, so that

$$\int_0^{\infty} p^2dp\,(\cdots) = \int\left(\overline{p}^2(z)\frac{dz}{z} - \overline{p}^2(\overline{z})\frac{d\overline{z}}{\overline{z}}\right) + 4i\mathrm{Re}\int\frac{p\,\mathrm{Im}\,z(p)}{z(p)}dp. \tag{2.31}$$

It is shown in Appendix B that the contribution of the second integral above is subleading, and we subsequently drop it. The first integral follows a contour from left to right just above the real z-axis, and returns from right to left just below. Since the distance from the contour to the axis behaves as $\mathcal{O}(T)$ near $z = 0$ and as $\mathcal{O}(T^2)$ away from $z = 0$, we can "pinch off" the contour into a clockwise contour encircling $z = 0$:

$$\int_0^\infty p^2 dp\,(\cdots) = \oint \overline{p}^2(z)\frac{dz}{z} = 2\pi i\,\overline{p}^2(0). \tag{2.32}$$

Thus we have

$$c(T) = \frac{1}{4\pi}\int_{-\infty}^{\infty} dy \frac{ye^y}{(e^y+1)^2}\overline{p}^2(0). \tag{2.33}$$

To evaluate this further, we need the solution of $p + 2\Sigma(p, \mu + yT - i\epsilon) - yT = 0$. It is shown in Appendix B that this quantity has the leading behavior

$$\lim_{\xi\to\mu} p(\xi) = k_F - \frac{1}{\pi^2(v_F^*)^2\alpha'}(\xi-\mu)\ln|\xi-\mu|. \tag{2.34}$$

Thus, to leading order,

$$c(T) = \frac{1}{4\pi}\int_{-\infty}^{\infty} dy \frac{ye^y}{(e^y+1)^2}\left(k_F^2 - \frac{2k_F}{\pi^2(v_F^*)^2\alpha'}yT\ln(yT)\right), \tag{2.35}$$

or

$$c(T) = -\frac{k_F}{6\pi(v_F^*)^2\alpha'}T\ln T. \tag{2.36}$$

2.4 Conclusions

We have shown that the exchange of transverse bosons can provide a pairing mechanism for Dirac CFs, allowing for the possibility of superconductivity in the half-filled Landau level, for angular momentum channels $|\ell| \geq 1$. Previous work [WC16b] could be criticized on three grounds: (a) the inclusion of the wave function renormalization (the Eliashberg-Z factor) was set to unity on the grounds that as long as there was a gap the qualitative phase diagram for quantum criticality could not be changed except perhaps close to the quantum critical point. (b) Therefore only one of the two Eliashberg equations was solved. It is now clear that qualitative results remain unchanged with insignificant numerical differences.

(c) The earlier work did not include the vertex correction. This could cast doubt on our results for the superconducting transitions at $T = 0$. Now we have shown that to a good approximation the vertex correction is identically zero, a far better situation than even in the electron-phonon problem. After all these corrections taken into account, we have shown that our previous results remain semiquantitatively correct, and there is no sign of pairing in the angular momentum channel $\ell = 0$. For the specific heat, our result of $c(T) \sim \frac{1}{e^2} T \ln T$ agrees strikingly with the result of [HLR93]; thus the specific heat cannot distinguish between Son's Dirac CF theory and HLR theory. As a by-product, the calculated self energy can be utilized in future work.

2.5 Supplementary material

2.5.1 Fermion self-energy

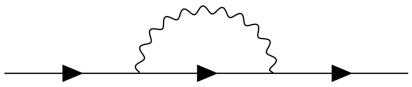

Figure 2.9: One-loop correction to fermion propagator

We would like to compute the one-loop Dirac CF self-energy, diagrammatically shown in Figure 2.9. Each vertex gives a factor of $i\gamma_i$, and we will use a corrected version of the boson propagator that takes into account screening from the finite density of fermions:

$$D(k, i\omega) P_{ij}^T(k) = \frac{8\pi}{\alpha'} \frac{1}{k + \frac{2k_F}{\alpha'} \frac{|\omega|}{k}} P_{ij}^T(k), \tag{2.37}$$

where $\alpha' \equiv \frac{e^2}{\epsilon_r}$ is the coupling of the original electrons in the problem, $P_{ij}^T(k) \equiv \delta_{ij} - \hat{k}_i \hat{k}_j$ is the transverse projector, and $k \equiv |\mathbf{k}|$. Importantly, the bosons are unscreened at small

ω/k; this leads to the anomalous behavior in the specific heat. We represent the fermion propagator by splitting it up into positive- and negative-energy parts as (see, e.g., [MSS01])

$$G(\mathbf{k}, i\omega_n) = \gamma_0 \sum_{s=\pm} G^{(s)}(\mathbf{k}, i\omega_n) P^{(s)}_{\mathbf{k}}, \tag{2.38}$$

where $P^{(s)}_{\mathbf{k}} \equiv \frac{1}{2}(1 + si\gamma_0 \vec{\gamma} \cdot \hat{k})$ is the projector onto the positive or negative energy bands, and

$$G^{(s)}(\mathbf{k}, i\omega_n) = \frac{1}{i\omega_n - s|\mathbf{k}| + \mu} \tag{2.39}$$

Then the relevant diagram gives the contribution

$$\Sigma(\mathbf{k}, i\nu_n) = \frac{1}{\beta^2} \sum_{r,m} \sum_{s=\pm} \int_p (i\gamma_i)\gamma_0 P^{(s)}_{\mathbf{k}} G^{(s)}(\mathbf{k}, i\xi_r) D(p-k, iz_m) P^T_{ij}(p) (\beta \delta_{\xi_r + z_m, \nu_n})(i\gamma_j). \tag{2.40}$$

Performing the sum over Matsubara frequencies, working out the matrix structure, and analytically continuing $i\nu_n \to \nu + i\epsilon$, we find that

$$\operatorname{Im} \Sigma'_R(\mathbf{k}, \nu) = -\frac{1}{2\pi} \sum_{s=\pm} s \int_p \int_\mu^\nu d\xi' \operatorname{Im} G^{(s)}_R(p, \xi') \operatorname{Im} D_R(k-p, \nu - \xi'), \tag{2.41}$$

where Σ' is defined in Equation (2.27). Now, we are interested in evaluating the self-energy on the Fermi surface, i.e. $|\mathbf{k}| \approx k_F$, $\nu \approx \mu$. In this limit, the region of frequency integration above is squeezed around $\xi' \approx \mu$, and we can simplify the fermion propagator:

$$\lim_{\xi' \to \mu} \operatorname{Im} G^{(s)}_R(p, \xi') = -\frac{\pi}{v^*_F} \delta(p - p(\xi')) \delta_{s,+}, \tag{2.42}$$

where $v^*_F \equiv |1 + \frac{\partial}{\partial p} \Sigma_R(p, \xi')|_{k_F}$, and $p(\xi')$ is defined as the solution to

$$\xi' + \mu - p - 2\operatorname{Re} \Sigma'_R(\mathbf{p}, \xi') = 0, \tag{2.43}$$

i.e. $p(\xi')$ is the momentum at the pole of the positive energy branch of the fermion propagator. Note that we have taken $\mu > 0$, and so the $s = -$ portion of the propagator does not contribute. With this substitution, it becomes clear that $\Sigma''_R = -\Sigma'_R$, and we now define $\Sigma_R \equiv \Sigma'_R$. Using this simplification, we can perform the angular integration of $\mathbf{p}$, to obtain

$$\operatorname{Im} \Sigma_R(\mathbf{k}, \nu) = \frac{1}{8\pi^2 v^*_F} \frac{1}{k} \int_\mu^\nu d\xi' p(\xi') \int_{|p(\xi') - k|}^{p(\xi') + k} dp \frac{\operatorname{Im} D_R(p, \nu - \xi')}{\sqrt{1 - \left[\frac{p^2 + k^2 - p^2(\xi')}{2pk}\right]^2}}. \tag{2.44}$$

Then, keeping only leading-order terms, these integrals can be performed, to obtain eventually

$$\operatorname{Im}\Sigma_R(\mathbf{k},\nu) = -\frac{1}{2\pi v_F^* \alpha'}(\nu-\mu)\tan^{-1}\left(\frac{\frac{2k_F}{\alpha'}(\nu-\mu)}{(k-k_F)^2}\right). \tag{2.45}$$

Here the limits $k \approx k_F$ and $\nu \approx \mu$ are understood. This expression contains the anomalous behavior on the Fermi surface.

We next show that this behavior of $\operatorname{Im}\Sigma_R$ leads to a logarithmic divergence of $\frac{\partial}{\partial\xi}\operatorname{Re}\Sigma_R(p,\xi)$ on the Fermi surface. We achieve this by means of the Kramers-Kronig relations, which give us, after an integration by parts,

$$\frac{\partial}{\partial\xi}\operatorname{Re}\Sigma_R(\mathbf{k},\xi) = \frac{\mathcal{P}}{\pi}\int_{-\infty}^{\infty} d\xi' \frac{\frac{\partial}{\partial\xi'}\operatorname{Im}\Sigma_R(\mathbf{k},\xi')}{\xi'-\xi}. \tag{2.46}$$

Substituting in Equation (2.45), and taking the principal part of the integral, we find that (up to finite terms)

$$\frac{\partial}{\partial\xi}\operatorname{Re}\Sigma_R(\mathbf{k},\xi) = \frac{1}{2\pi v_F^*\alpha'}\ln(\xi-\mu). \tag{2.47}$$

Now, differentiating Equation (2.43), and substituting in Equation (2.47), we see that

$$\frac{dp(\xi)}{d\xi} = \frac{1}{v_F^*}\left(1 - \frac{1}{\pi v_F^*\alpha'}\ln(\xi-\mu)\right). \tag{2.48}$$

Finally, we can integrate this and drop subleading terms to obtain

$$p(\xi) = k_F - \frac{1}{\pi(v_F^*)^2\alpha'}(\xi-\mu)\ln(\xi-\mu). \tag{2.49}$$

2.5.2 Vertex correction

Here we can make use of the Ward identity, as in [CNS95], which gives us the vertex correction Γ in terms of the self-energy:

$$\hat{\mathbf{k}}\cdot\nabla_{\mathbf{k}}\Sigma(k,\mu)|_{k_F} = \Gamma(k_F,k_F,\mu). \tag{2.50}$$

Since our entire model is a low-energy theory, we only care about the vertex correction at the Fermi surface. Using Equation (2.45), we can compute the derivative of the self-energy:

$$\operatorname{Im}\hat{\mathbf{k}}\cdot\nabla_{\mathbf{k}}(k,\nu) \propto \frac{(\nu-\mu)^2(k-k_F)}{\left(\frac{2k_F(\nu-\mu)}{\alpha'}\right)^2 + (k-k_F)^4}. \tag{2.51}$$

This vanishes on the Fermi surface, so that $\mathrm{Im}\,\Gamma(k_F, k_F, \nu) = 0$. Similarly, using the Kramers-Kronig relations to obtain the real part of the self-energy, we also find that $\mathrm{Re}\,\Gamma(k_F, k_F, \nu) = 0$, so that

$$\Gamma^{(2)}(k_F, k_F, \mu) = 0. \tag{2.52}$$

This justifies the use of the Eliashberg equations in this problem, and also justifies the use of Luttinger's expansion of the thermodynamic potential, Equation (2.25).

CHAPTER 3

Ferromagnetism in the Overdoped Cuprates

3.1 Introduction

The elucidation of the phase diagram for high-temperature superconducting materials has been one of the central driving forces in condensed matter physics for the last few decades; see Figure 1.1. Much of the focus has been on the underdoped portion of the phase diagram close to the Mott insulating antiferromagnetic state, due to the relative ease of preparing samples at low doping. The conventional wisdom has been that the state beyond the superconducting dome is a Fermi liquid, which wisdom has received some experimental support [PBH02, HAN03, NBM03]. These results are not unambiguous, as pointed out in [KGC07], and furthermore experiments find a sharp upturn in magnetic susceptibility at high doping that poses serious problems for the Fermi liquid picture [TII89, ONK91, KSM91, THM92, NOM94, WBK05]. It was thus conjectured by Kopp, Ghosal, and Chakravarty that the overdoped terminus of the superconducting dome is a quantum critical point separating the superconducting phase from a *ferromagnetic* phase, offering an explanation for the magnetic susceptibility measurements [KGC07].

In the years since, there have been several experiments supporting the existence of ferromagnetic order in the overdoped cuprates. μSR measurements have found dilute static magnetic moments below ~ 1 K in $La_{2-x}Sr_xCuO_4$ at a hole doping of $x = 0.33$, indicative of weak itinerant ferromagnetism in which the dopants are pinned to Cu atoms, but did not find long-range magnetic order [SKP10]. The same experiment detected a crossover between $\rho_{ab} \sim T^2$ and $\rho_{ab} \sim T^{5/3}$ dependence with an increase in temperature, consistent with behavior seen in the weak three-dimensional itinerant ferromagnet Y_4Co_3 [KS00]. Quan-

tum critical scaling behavior was detected in electron-doped $La_{2-x}Ce_xCuO_4$ (LCCO), with a normal-state resistivity of $\rho_{ab} \sim T^{1.6}$ near the end of the dome, and $\rho_{ab} \sim T^{4/3}$ dependence was seen in $(Bi,Pb)_2Sr_2CuO_{6+\delta}$ doped beyond the superconducting dome [KAS18], a signature of two-dimensional itinerant ferromagnetism [MK73, UM75, HM95], alongside an enhancement of the Wilson ratio, a further indication of ferromagnetic order. Most recently, magnetic transport and polar Kerr effect measurements on electron-doped LCCO thin films have provided strong evidence of itinerant ferromagnetic behavior beyond the superconducting dome below ~ 4 K [SWZ20].

With this evidence in mind, we explore the possibility of a ferromagnetic ground state in the heavily-overdoped single-band Hubbard model. In Section 3.2 we do so by directly comparing the energies of a ferromagnetic state and a singlet gas, and in Section 3.3 we do so by numerically computing the ground state energy of several mean-field ansatze. We find that ferromagnetism is indeed plausible in the relevant regime of doping and parameter space.

First some comments about the Hubbard model, and the physics one might expect to find. The simplest single-band Hubbard model is defined as

$$H = -t \sum_{\langle ij \rangle, \sigma} c^\dagger_{i\sigma} c_{j\sigma} + U \sum_i n_{i\uparrow} n_{i\downarrow}, \tag{3.1}$$

where $c_{i\sigma}$ are fermion operators at site i of spin $\sigma = \pm$ living on a two-dimensional square lattice, $\langle ij \rangle$ indicate nearest-neighbor sites, $n_{i\sigma}$ is the fermion number operator on site i, and $t > 0$ and $U > 0$ are energy scales. One may extend this model to include next nearest-neighbor coupling, etc. This model describes spin-1/2 fermions hopping around on a lattice, interacting through an on-site repulsive interaction U, which can be considered as a toy model of the Coulomb interaction. One can immediately see that if $U = 0$, the Hamiltonian can be diagonalized in the momentum basis, and a wave-like description of the fermions is appropriate; if $t = 0$, the Hamiltonian is diagonal in position space, and a particle-like description of the fermions is appropriate. Thus with t and U non-zero, the Hubbard model describes a competition between the wave-like nature of free fermions and the particle-like nature of the stationary interacting fermions. Much of the rich physics of the Hubbard model

can be understood in terms of this competition.

So, what sort of ground state can we expect this model to support? We need to mention immediately that at nonzero temperature, the Mermin-Wagner theorem precludes long-range order, so we will restrict our consideration to $T = 0$; in the cuprates, even though we focus on a single copper-oxide plane, inter-layer coupling stabilizes order by making the system "three-dimensional enough" so that order is possible at finite T. Let's first consider the case in which there are half as many fermions as lattice sites; this is referred to as half-filling, since each site can hold as many as two fermions. If one simply considers a two-site lattice, the Hilbert space is six-dimensional and can be exactly diagonalized, and the ground state is found to be antiferromagnetic for any $U > 0$. This result generalizes to the full lattice, and thus at half-filling the ground state of the Hubbard model is an antiferromagnet. Due to the on-site Coulomb repulsion, this ground state doesn't conduct upon application of a small electric field, and so this state is a Mott insulator. This is congruent with what we find for the undoped parent compounds of high-T_c superconductors, which indicates that the problem of understanding the phase diagram of such superconductors is related to the problem of finding the ground state of the doped Hubbard model [LNW06]. It is noteworthy that a magnetically-ordered ground state is the result of the conspiracy between the Pauli exclusion principle and a *spin-independent* interaction term, whereas the exclusion principle itself only ever leads to paramagnetism.

What happens away from half-filling? It is known that at infinite U, doping away from half-filling by even a single hole drives the antiferromagnetic phase at half-filling to ferromagnetism, a mechanism known as Nagaoka ferromagnetism [Nag66]. It is suspected, but not rigorously proven, that at large finite U a larger amount of doping will still lead to such ferromagnetism. The appearance of both antiferromagnetic and ferromagnetic ground states in the Hubbard model indicates that this model may be rich enough to include the various universality classes of states of interest in real physical systems, despite its superficial simplicity, and thus justifies itself as worthy of our attention. It is hoped that an understanding of the phase diagram of this model will provide insight into the phase diagram of the high-T_c

cuprate superconductors.

3.2 Ferromagnetism vs. Dilute Electron Gas

Consider the Hamiltonian of the 2D, single-band Hubbard model

$$H = H_0 + H_U = \sum_{k,\sigma} E(k) c^\dagger_{k\sigma} c_{k\sigma} + U \sum_i n_{i\uparrow} n_{i\downarrow} \tag{3.2}$$

with $E(k)$ some band energy. Our goal will be to compare the energies of two states: a dilute singlet gas and a uniformly polarized state.

We begin by computing the energy of a dilute singlet gas (representative of a paramagnetic state) using scattering theory, following [Mat81]. We can see that the singlet state $|\psi_{k,k'}\rangle \equiv \frac{1}{\sqrt{2}}(c^\dagger_{k\uparrow} c^\dagger_{k'\downarrow} - c^\dagger_{k\downarrow} c^\dagger_{k'\uparrow})|0\rangle$, unlike the triplet states, is not an eigenstate of H_U, and thus of the full Hubbard Hamiltonian:

$$H_U|\psi_{k,k'}\rangle = \frac{U}{N}|\psi_{k,k'}\rangle + \frac{U}{N}\sum_{q\neq 0}|\psi_{k+q,k'-q}\rangle. \tag{3.3}$$

We can obtain the eigenstate $|\Psi_{k,k'}\rangle$ of energy $W_{k,k'}$ of the full Hamiltonian in scattering theory, imagining an incoming singlet state scattering off of the on-site Coulomb potential:

$$|\Psi_{k,k'}\rangle = |\psi_{k,k'}\rangle + \frac{1}{N}\sum_{q\neq 0} f_q |\psi_{k+q,k'-q}\rangle. \tag{3.4}$$

The goal is to compute the coefficients f_q. We can write down the Schrodinger equation $H|\Psi_{k,k'}\rangle = W_{k,k'}|\Psi_{k,k'}\rangle$, and equate the coefficients of $|\psi_{k,k'}\rangle$ to obtain the energy eigenvalue

$$W_{k,k'} = E_{k,k'} + \frac{U}{N}\left(1 + \frac{1}{N}\sum_{q\neq 0} f_q\right), \tag{3.5}$$

where $E_{k,k'} \equiv E_k + E_{k'}$ is the energy of the triplet states and E_k is the single-particle energy. We can equate the coefficients of $|\psi_{k+q,k'-q}\rangle$ and rearrange to obtain

$$f_q = \frac{U}{(W_{k,k'} - E_{k+q,k'-q})}\left(1 + \frac{1}{N}\sum_{q'} f_{q'}\right). \tag{3.6}$$

We can solve this by summing over all q:

$$\sum_q f_q = \left(1 + \frac{1}{N}\sum_{q'} f_{q'}\right) \sum_q \frac{U}{(W_{k,k'} - E_{k+q,k'-q})}, \tag{3.7}$$

which we can solve for $\sum_q f_q$, after defining $G_0 \equiv -\frac{1}{N}\sum_q \frac{1}{(W_{k,k'} - E_{k+q,k'-q})}$:

$$\sum_q f_q = \frac{-NG_0U}{1 + G_0U}. \tag{3.8}$$

Combining Equations (3.6) and (3.8), we can solve for f_q:

$$f_q = \frac{1}{(W_{k,k'} - E_{k+q,k'-q})} \frac{U}{1 + UG_0}. \tag{3.9}$$

This allows us to write down an equation for the full eigenvalue

$$W_{k,k'} = E_{k,k'} + \frac{1}{N} t(W_{k,k'}), \quad t(W_{k,k'}) \equiv \frac{U}{1 + UG_0}. \tag{3.10}$$

So far, this calculation is exact; we will decouple this by taking $t(W_{k,k'}) \approx t(E_{k,k'})$.

Now let's consider a dilute gas of singlet pairs. In this case, the k scattering integrals must be restricted to unoccupied states, outside of the Fermi sea. Then we have an effective Hamiltonian for singlet pairs:

$$H_{\text{sing}} = \sum_{k,\sigma} E(k) n_{k\sigma} + \frac{1}{N}\sum_{k,k'} \tilde{t}(E_{k,k'}) n_{k\uparrow} n_{k'\downarrow}, \tag{3.11}$$

where a tilde over a quantity indicates that any momentum-space sum inside is restricted to values such that $E_{k+q} < E_F$ and $E_{k'-q} < E_F$. If the gas is sufficiently dilute, the band energy can be approximated by the effective-mass energy $E(k) = \frac{\hbar^2 k^2}{2m^*}$. Then the kinetic energy per spin component is given by

$$T \equiv \sum_{k<k_F} = N \frac{d}{d+2} W \rho^{\frac{d+2}{d}}, \tag{3.12}$$

where we define the bandwidth $W \equiv \frac{\hbar^2 k_0^2}{2m^*}$, and the number of electrons per atom in a given spin direction is $\rho \equiv (k_F/k_0)^d$, and $k_0 \equiv 2\pi/a$ with lattice spacing a. We can compute the remaining energy by evaluating

$$\tilde{G}_0 = \frac{V}{W} \int_{|\mathbf{k}+\mathbf{q}|>k_F, |\mathbf{k}'-\mathbf{q}|>k_F, q<k_0} \frac{d^d q}{(2\pi)^d} \frac{k_0^2}{(\mathbf{k}+\mathbf{q})^2 + (\mathbf{k}'-\mathbf{q})^2 - k^2 - k'^2}. \tag{3.13}$$

In the dilute approximation, the singlets only fill up states with $k, k' \ll k_0$; we can thus approximate the above with

$$\tilde{G}_0 \approx \frac{a^d}{W} \int_{q>k_F, q<k_0} \frac{d^d q}{(2\pi)^d} \frac{k_0^2}{2q^2}. \tag{3.14}$$

Now we specialize to $d = 2$, and obtain

$$\tilde{G}_0 = -\frac{1}{W} \log(\rho), \tag{3.15}$$

Then the scattering contribution to the energy is

$$N \frac{U}{1 + U\tilde{G}_0} \frac{\sum_{k,k'<k_F} 1}{\sum_{k,k'<k_0} 1} = N \frac{U\rho^2}{1 + U\tilde{G}_0}, \tag{3.16}$$

and the total energy is then

$$E_{\text{sing}} = NW\rho^2 (2 \cdot \frac{1}{2} + \frac{U}{W - U \log \rho}). \tag{3.17}$$

By contrast, the total energy of a fully ferromagnetic state is given by

$$E_{\text{polarized}} = \frac{1}{2} NW(2\rho)^2 = 2NW\rho^2, \tag{3.18}$$

and thus

$$E_{\text{polarized}} - E_{\text{sing}} = NW\rho^2 \left(1 - \frac{U}{W + U|\log \rho|}\right). \tag{3.19}$$

We can see that the criterion for ferromagnetism is then

$$\frac{1}{W/U + |\log \rho|} > 1. \tag{3.20}$$

In the limit $U/W \to \infty$, this inequality becomes $\rho > e^{-1} \approx 0.3679 \equiv \rho_c$. Rewriting this in terms of the doping parameter $x = 1 - \rho$, we arrive at the main result of this section,

$$x < 1 - \rho_c e^{W/U}. \tag{3.21}$$

This result gives the doping for which the ferromagnetic state is of lower energy than the dilute singlet gas. Since the model we use is particle-hole symmetric, x can correspond either to electron doping or to hole doping.

Experiments indicate a ratio $U/W \sim 2.5$, at which the criterion for ferromagnetism is $x < 0.451$ in our approximation. This is well within the regime of interest at the far end of the superconducting dome.

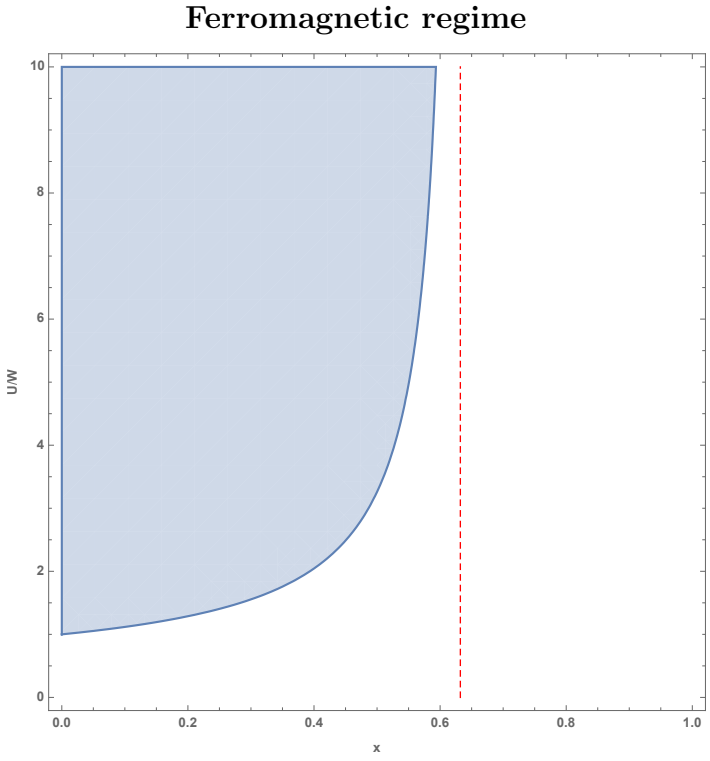

Figure 3.1: For the shaded region, the energy of a spin-polarized state is lower than the energy of a dilute gas of singlets. Here U is the Hubbard U, W is the bandwidth, and x is the electron or hole doping ($x = 0$ corresponds to 1 electron per atom). Above a critical doping of $x = 1 - e^{-1}$, no ferromagnetism is possible in this approximation. Corrections to the dilute gas approximation should not change the qualitative nature of this diagram. Note that this does *not* indicate that one should find a ferromagnetic state at half-filling, where the ground state is certainly an antiferromagnetic Mott insulator; this is simply a comparison of the energies of a ferromagnetic state and a singlet gas.

3.3 Mean-field phase diagram

In this section we use mean field theory to determine the phase diagram of the 2D Hubbard model, in the spirit of [LW07]. The Hubbard Hamiltonian after mean-field decoupling is

$$H = \sum_{k\sigma}(\epsilon_k - \mu - U(n-1)/2)n_{k\sigma} + U\sum_i(\langle n_{i\uparrow}\rangle n_{i\downarrow} + \langle n_{i\downarrow}\rangle n_{i\uparrow} - \langle n_{i\uparrow}\rangle\langle n_{i\downarrow}\rangle) + U/4. \quad (3.22)$$

Moving forward, we absorb the term $U(n-1)/2$ into the chemical potential. Here $\epsilon_k = -2t(\cos k_x + \cos k_y) + 4t_2 \cos k_x \cos k_y$ includes both nearest neighbor and next-nearest neighbor hopping terms, which breaks the particle-hole symmetry of the Hamiltonian. Different phases correspond to different choices of $\langle n_{i\sigma}\rangle$, which for ordered states correspond to the order parameter. To determine the phase diagram, we we compute the total energy of various choices of $\langle n_{i\sigma}\rangle$ as a function of doping, solving for the order parameter self-consistently as needed, and choose the one with the lowest energy as the ground state. A typical plot of the ground state energies is shown in Fig. 3.2.

3.3.1 Paramagnet

In the paramagnetic state, $n = 2\langle n_{i\uparrow}\rangle = 2\langle n_{i\downarrow}\rangle$, so that

$$H = \sum_{k\sigma}(\epsilon_k - \mu)n_{k\sigma} - \frac{1}{4}UN(n-1)^2, \quad (3.23)$$

where we have again absorbed some terms into the definition of μ. Thus the density and energy per site are

$$\begin{aligned} n &= \frac{2}{N}\sum_k f(E_k) \\ f &= \frac{2}{N}\sum_k E_k f(E_k) - \frac{1}{4}U(n-1)^2, \end{aligned} \quad (3.24)$$

where $E_k \equiv \epsilon_k - \mu$, and $f(E_k)$ is the Fermi-Dirac distribution, $f(x) = 1/(1+e^{\beta x})$. There is no order parameter for the paramagnetic state.

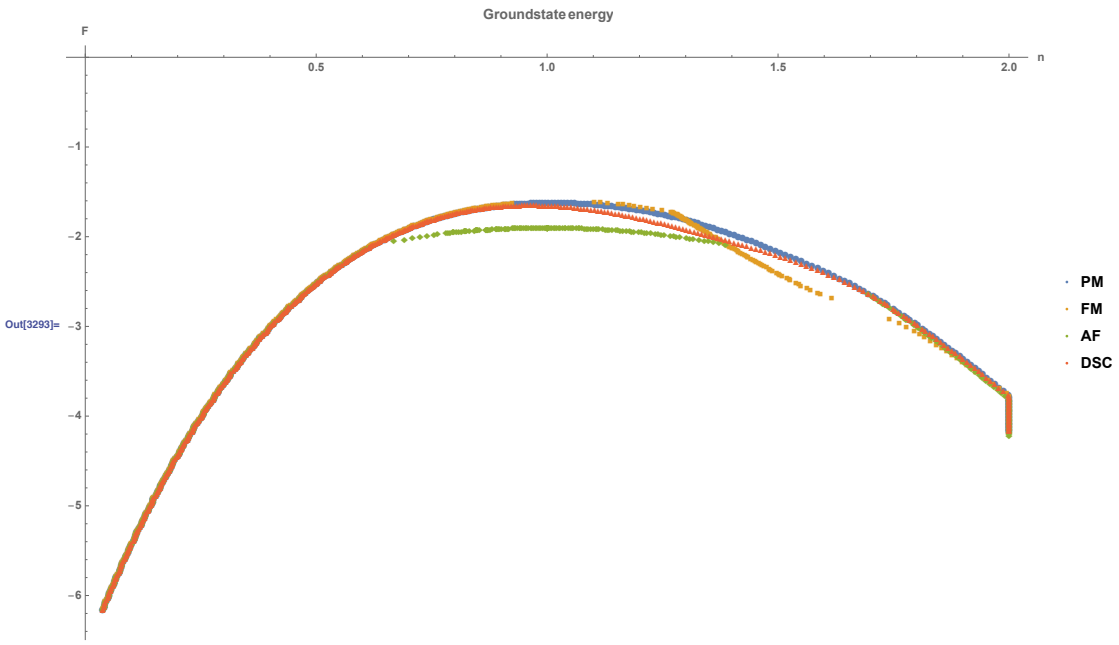

Figure 3.2: An example of the ground state energy F, in units of t, as a function of average electron number per site n. This example was taken at $U = 5$. The phase boundaries at a particular value of U are drawn where the lowest curves cross.

3.3.2 Ferromagnet

In the ferromagnetic state, we have $\langle n_{i\sigma}\rangle = \frac{1}{2}n + \sigma m$. Then we have

$$H = \sum_{k\sigma}(\epsilon_k - \mu - U\sigma m)n_{k\sigma} - UN\left(\frac{(n-1)^2}{4} - m^2\right). \tag{3.25}$$

The energy per site is thus

$$f = \frac{1}{N}\sum_k [E_{k\uparrow}f(E_{k\uparrow}) + E_{k\downarrow}f(E_{k\downarrow})] - U\left(\frac{(n-1)^2}{4} - m^2\right), \tag{3.26}$$

where $E_{k\sigma} \equiv \epsilon_k - \mu - U\sigma m$. The equation determining m is $\partial f/\partial m = 0$, or

$$m = \frac{1}{2N}\sum_k [f(E_{k\uparrow}) - f(E_{k\downarrow})]. \tag{3.27}$$

Note that this is the same as $m = \frac{1}{2}(\langle n_{i\uparrow}\rangle - \langle n_{i\downarrow}\rangle)$, which is what we expect for the ferromagnetic order parameter. The self-consistent equations are thus

$$\begin{aligned} n &= \frac{1}{N}\sum_k [f(E_{k\uparrow}) + f(E_{k\downarrow})] \\ m &= \frac{1}{2N}\sum_k [f(E_{k\uparrow}) - f(E_{k\downarrow})] \end{aligned} \tag{3.28}$$

3.3.3 Antiferromagnet

In the case of the antiferromagnetic state, we have $\langle n_{i\sigma}\rangle = \frac{1}{2}n + \sigma(-1)^{i_x+i_y}s$. Thus

$$H = \sum_{k\sigma}(\epsilon_k - \mu)c^\dagger_{k\sigma}c_{k\sigma} - Us\sum_k (c^\dagger_{k,\uparrow}c_{k+Q,\uparrow} - c^\dagger_{k,\downarrow}c_{k+Q,\downarrow}) - NU\left(\frac{(n-1)^2}{4} - s^2\right). \tag{3.29}$$

We can rewrite this in Nambu form as

$$H = \sum_{\{k\}\sigma} \Psi^\dagger_{k\sigma} \begin{pmatrix} \epsilon_k - \mu & -Us\sigma \\ -Us\sigma & \epsilon_{k+Q} - \mu \end{pmatrix} \Psi_{k\sigma} - NU\left(\frac{(n-1)^2}{4} - s^2\right), \tag{3.30}$$

with $\Psi^\dagger_{k\sigma} = (c^\dagger_{k\sigma}, c^\dagger_{k+Q,\sigma})$, and $\{k\}$ is the half of the Brillouin zone bounded by $|k_x \pm k_y| = \pi$. The matrix above has eigenvalues

$$E^\pm_{k\sigma} = -\mu + 4t_2\cos k_x \cos k_y \pm \sqrt{(Us)^2 + (2t(\cos k_x + \cos k_y))^2}. \tag{3.31}$$

Thus the energy per site is

$$f = \frac{2}{N}\sum_{\{k\}}(E^+_{k\sigma}f(E^+_{k\sigma}) + E^-_{k\sigma}f(E^-_{k\sigma})) - U\left(\frac{(n-1)^2}{4} - s^2\right), \tag{3.32}$$

where $\tilde{E}_k \equiv \sqrt{(Us)^2 + (2t(\cos k_x + \cos k_y))^2}$. The equation determining s is $\partial f/\partial s = 0$, or

$$s = -\frac{Us}{N}\sum_{\{k\}}\frac{f(E^+_{k\sigma}) - f(E^-_{k\sigma})}{\tilde{E}_k}, \tag{3.33}$$

and the density is set by

$$n = \frac{2}{N}\sum_{\{k\}}[f(E^+_{k\sigma}) + f(E^-_{k\sigma})]. \tag{3.34}$$

The above two equations are to be solved self-consistently. The results of this analysis are included in Fig. 3.3, as a comparison to an analogous figure in [LW07].

3.3.4 *d*-wave superconductor

For the *d*-wave superconductor, we take as our starting point the effective Hamiltonian of Bogoliubons, plus a term from the Hubbard Hamiltonian:

$$\begin{aligned} H &= \sum_{k\sigma} E_k \gamma^\dagger_{k\sigma}\gamma_{k\sigma} + E_0 - U(n-1)^2/4 \\ E_0 &= \sum_k (\epsilon_k - \mu - E_k) + J\Delta^2 \\ E_k &= \sqrt{(J\Delta(\cos k_x - \cos k_y))^2 + (\epsilon_k - \mu)^2}. \end{aligned} \tag{3.35}$$

The ground state energy has no quasiparticles and is simply $E_0 - U(n-1)^2/4$, and we can find the gap equation by minimizing E_0 with respect to Δ:

$$\Delta = J\sum_k \frac{\Delta(\cos k_x - \cos k_y)^2}{E_k}. \tag{3.36}$$

For the system density, we use the same as the paramagnetic state,

$$n = \frac{2}{N}\sum_k f(\epsilon_k - \mu). \tag{3.37}$$

This is not strictly correct, but should not affect the structure of the phase diagram too strongly. The results of this analysis are shown in Fig. 3.4.

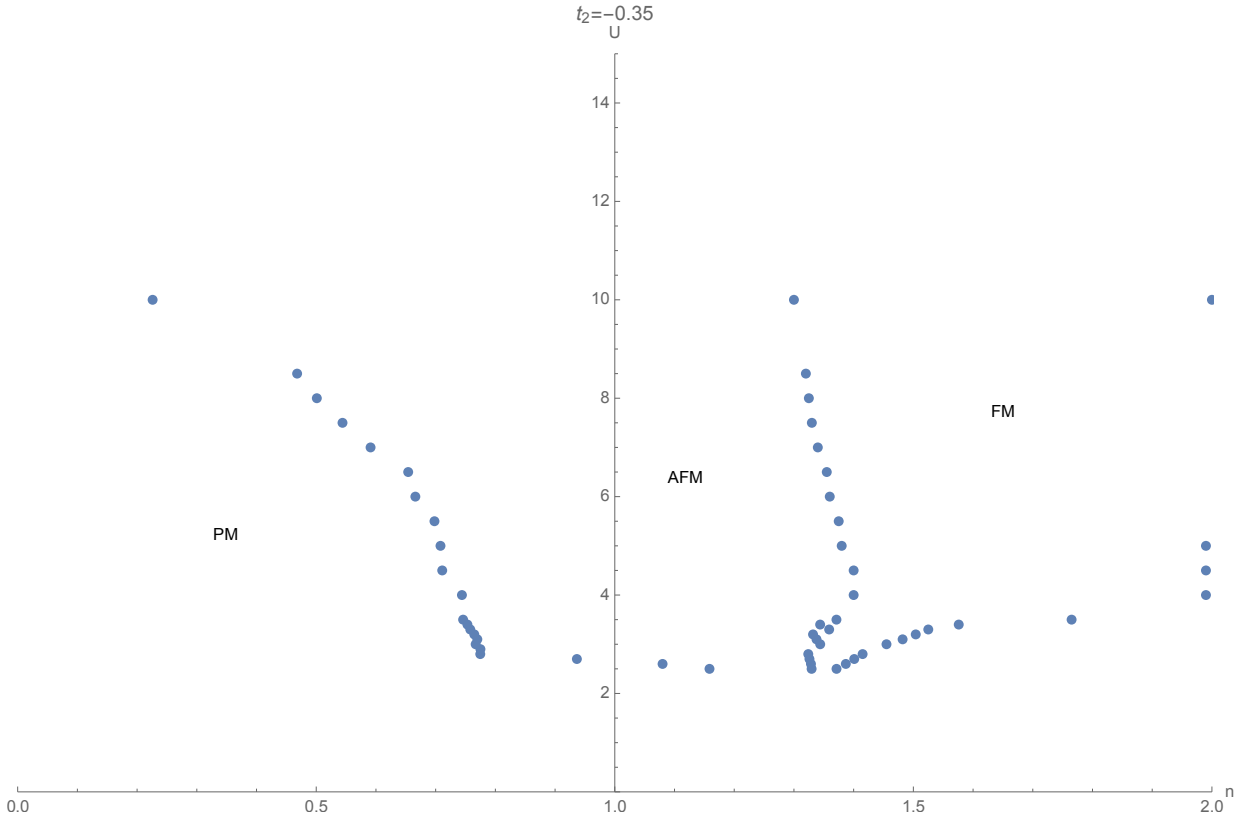

Figure 3.3: Mean-field phase diagram of the 2D single-band Hubbard model with $t_2 = -0.35t$. Here U is in units of t, and n is the number of electrons per atom. Compare to Fig. 2 of [LW07]; our seems to be reflected across the y-axis, for reasons unknown to us. The ferromagnetic portion of the phase diagram persists all the way to the fully-occupied lattice, in contrast to the dilute-gas result presented in the previous section, which indicated that no ferromagnetism was possible above $n \approx 1.45$.

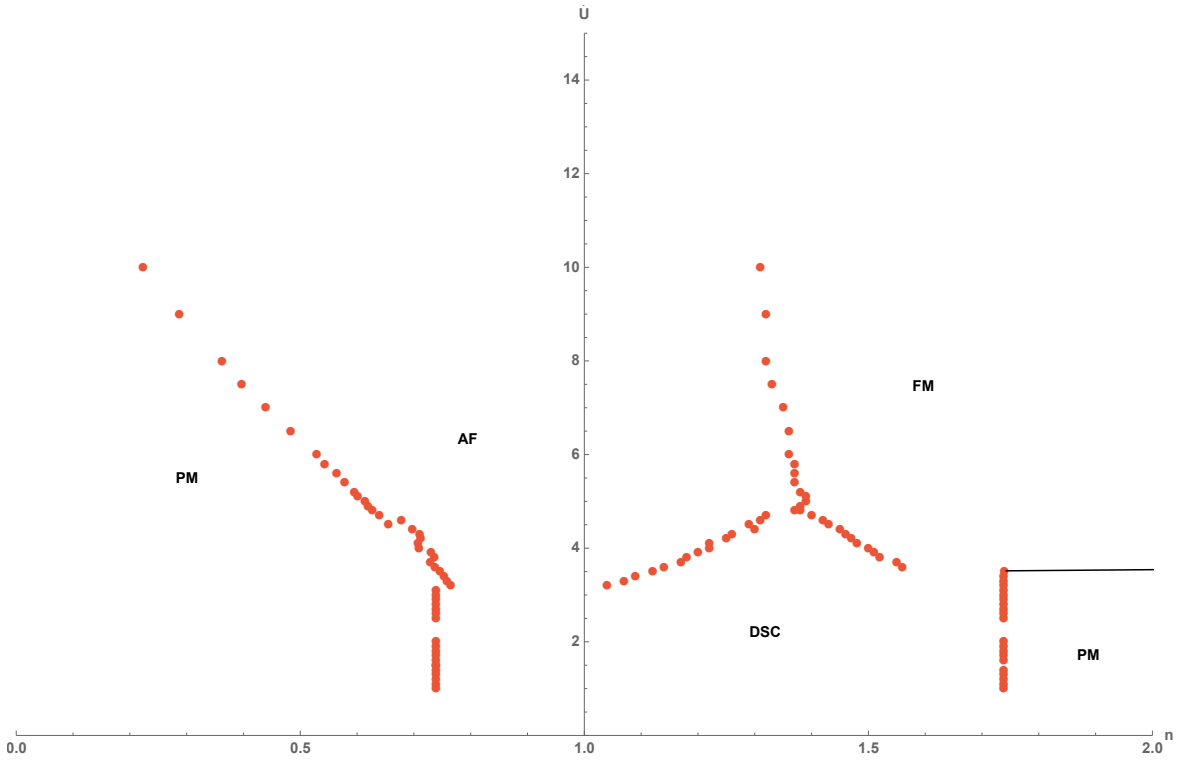

Figure 3.4: Mean-field phase diagram of the 2D single-band Hubbard model with $t_2 = -0.35t$, including the d-wave superconducting order parameter. Here U is in units of t, and n is the number of electrons per atom. We can see the superconducting region at small U. It makes contact with the FM region around a hole doping of ~ 0.5 with these parameters. It is possible that with this model, the superconducting region should really span the entire doping region at small U, but we cut it off where the computer gave a gap of zero to the precision used.

In summary, we have found that it is reasonable to expect ferromagnetic behavior at low temperatures near the overdoped end of the superconducting dome, using both perturbation theory and mean-field theory in the two-dimensional single-band Hubbard model.

CHAPTER 4

Dzyaloshinskii-Moriya interactions from density waves

Portions of this chapter are adapted from the publication:

Powell, I. E., Durr, S., Rombes, N. and Chakravarty, S. *Density Wave Mediated Dzyaloshinskii-Moriya Interactions.* In preparation.

4.1 Introduction

Despite concerted efforts to illuminate the precise nature of the pseudogap phase of the cuprate high-temperature superconductors[Var99, Var06, YRZ06, NPK07], it remains unclear which of a host of competing order parameters is responsible for the interesting behavior of this phase. One promising candidate[CLM01] is the $\ell = 2$ spin-singlet order, the d-density wave (DDW), which gives rise to a $d_{x^2-y^2}$ gap and currents that alternate between adjacent plaquettes on a square lattice. The relevance of this state is certainly believable given the proximity of the pseudogap phase to the antiferromagnetic Mott insulator at low doping, which doubles the Brillouin zone in the same way and is susceptible to singlet pairing.

This density wave state of nonzero angular momentum belongs to a larger class of such states[Nay00], and it is worth exploring other, more exotic members of this class related to the singlet DDW which maintain the key characteristics necessary for relevance to the pseudogap phase. Such states are also of some interest due to their topological properties.[HRC11] We focus on a mixed triplet-singlet DDW order, which has generated interest recently due to

promising transport calculations consistent with surprising physics found in the pseudogap phase of the cuprate superconductor $La_{2-x}Sr_xCuO_4$ and related compounds.[GLB19, LL19] Namely, for nonzero hole doping, the mixed triplet-singlet DDW state generates a nonvanishing thermal Hall conductivity κ_{xy}, and hosts hole pockets on the reduced Brillouin zone boundaries consistent with Hall coefficient measurements.[CK08, DCL10]

At the mean-field level a general density wave state may be described by the Hamiltonian

$$H_{\text{DDW}} = \sum_{\mathbf{k},\mathbf{Q}} c^\dagger_{\mathbf{k}+\mathbf{Q}} [\Phi^\mu_{\mathbf{Q}}(\mathbf{k})\tau^\mu] c_{\mathbf{k}} + \text{h.c.}, \tag{4.1}$$

where $\mathbf{Q}$ is the wave vector at which the density wave condensation occurs; τ^1, τ^2, and τ^3 are the Pauli matrices; and $\tau^0 = \mathbb{I}_2$. This Hamiltonian can be thought of as arising from a mean-field decomposition of the most general interacting problem[Lau14, NJK99, Sch89, KK03] in which the order parameter

$$\langle c^\dagger_{\mathbf{k}+\mathbf{Q},\alpha} c_{\mathbf{k},\beta} \rangle = [\Phi^\mu_{\mathbf{Q}}(\mathbf{k})\tau^\mu]_{\alpha\beta} \tag{4.2}$$

acquires a nonzero value for some nonzero $\mathbf{Q}$. In our work we assume that all terms which transform nontrivially under rotations and translations are captured by this mean-field decomposition.

Here we consider a specific example of Eq. (4.1), namely the the triplet-singlet DDW wave[HRC11] (denoted $i\sigma d_{x^2-y^2} + d_{xy}$)

$$\begin{aligned} \Phi^i_{\mathbf{Q}}(\mathbf{k}) &\propto iW_0 N_i (\cos k_x - \cos k_y) \\ \Phi^0_{\mathbf{Q}}(\mathbf{k}) &\propto \Delta_0 \sin k_x \sin k_y, \end{aligned} \tag{4.3}$$

where N_i is a unit vector pointing along the spin quantization direction, $i = 1, 2, 3$, and $\mathbf{Q} = (\pi/a, \pi/a)$. This model was shown by Z-X. Li & D-H. Lee to produce a nonzero thermal Hall effect, shown here in Figure 4.1. In real space the Hamiltonian is written as

$$H_{\text{DDW}} = H_t + H_s \tag{4.4}$$

with

$$\begin{aligned} H_t = \frac{iW_0}{4} \sum_{i,\alpha,\beta} (-1)^{m+n} (\mathbf{N}\cdot\boldsymbol{\sigma})_{\alpha\beta} \\ \times [c^\dagger_{i+a\hat{x},\alpha} c_{i,\beta} - c^\dagger_{i+a\hat{y},\alpha} c_{i,\beta}] + \text{h.c.} \end{aligned} \tag{4.5}$$

and

$$H_s = \frac{\Delta_0}{2} \sum_{i,\alpha,\beta} \delta_{\alpha,\beta} (-1)^{m+n} \times \left[c^\dagger_{i+a\hat{x}+a\hat{y},\alpha} c_{i,\beta} - c^\dagger_{i+a\hat{x}-a\hat{y},\alpha} c_{i,\beta} \right] + \text{h.c.}. \tag{4.6}$$

The Hamiltonian $H_0 + H_{\text{DDW}}$, describes a topological Mott insulator[Nay00, HRC11] with a quantized spin Hall conductance; it is a variant of the singlet d-density wave model hypothesized[CLM01] to explain the pseudogap phase of the cuprates. Unlike the singlet d-density state, however, the mixed triplet-singlet $i\sigma d_{x^2-y^2} + d_{xy}$-density wave state does not inherently break time reversal symmetry, yet it retains most of the signatures of the singlet d-density wave state. For example, the $i\sigma d_{x^2-y^2} + d_{xy}$-density wave wave state possesses hole pockets centered along the Brillouin zone diagonals which are consistent with both the measured Hall coefficient[GLB19] and some aspects of quantum oscillation experiments[DPL07, SHP08, WC16a]. Recently, second-harmonic generation experiments have suggested that an inversion symmetry breaking is responsible for large second harmonic generation signatures in $YBa_2Cu_3O_y$[ZBL16] but we note that this could be due to, in principle, the quadrupole moment induced via a triplet d-density wave[Nay00], and the spatial reflection symmetry breaking caused by the d_{xy} term.

We now ask ourselves, what effect does this density wave state have on the localized spins of the lattice? The magnitude of the experimentally-measured thermal Hall effect exceeds the maximum possible contribution from the density wave state alone by almost an order of magnitude[LL19]; it is possible that magnetic excitations induced by the density wave state could contribute further. In our work we assume that at nonzero doping, density wave fluctuations will exist even when the material in question is in a magnetically ordered phase. The triplet part of the density wave order parameter induces a staggered spin current[NJK99] on the lattice, and hence, for neighboring lattice points A and B, this intrinsic spin current implies that there exists no center of inversion at any point C on the bond connecting A and B, thereby allowing an antisymmetric exchange among the localized spins.[KKA16, Tat19] These types of antisymmetric exchanges have been considered in the literature[KH19], but to our knowledge have never been considered in the context of being generated via intrinsic

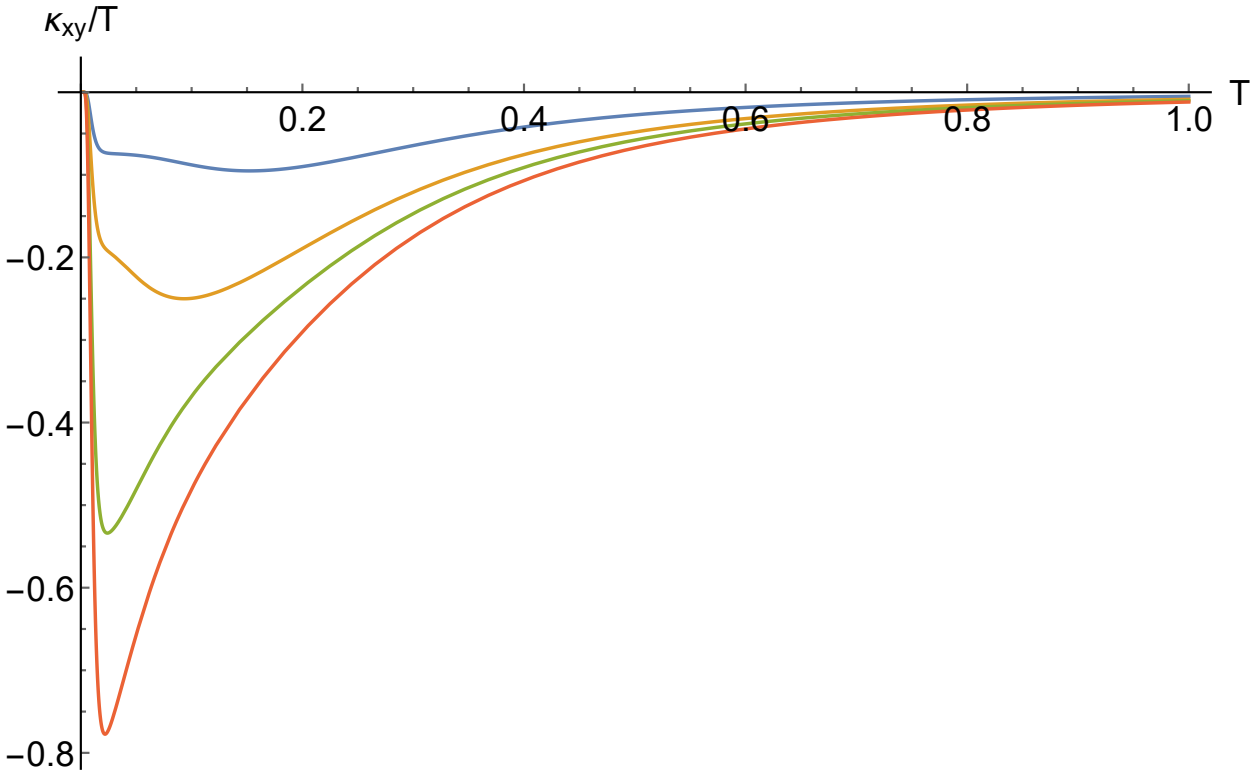

Figure 4.1: Thermal Hall conductivity κ_{xy}/T as a function of temperature T produced by the triplet-singlet DDW state defined by Equation (4.3) with $\Delta_0 = 0.5t$, magnetic field $B = 0.1t/\mu_B$, and doping $p = 0.06$. Blue, orange, green, and red curves correspond to $W_0 = 0.15t, 0.35t, 0.55t$, and $0.75t$, respectively. κ_{xy} has units of $k_B^2/\hbar$

spin currents.

We find that the spin currents intrinsic to the triplet flavored density wave states induce a Dzyaloshinskii-Moriya (DM) interaction between the underlying neighboring spins[KKA16], and we investigate the effect that this DM interaction has on antiferromagnetic and ferromagnetic spin textures, using both Holstein-Primakoff and Schwinger boson mean-field theories. It has been previously demonstrated[SCS19, HPL19, KH19] that certain DM interactions can lead to a thermal Hall effect. We find that the particular DM interaction induced by triplet-singlet DDW states can not contribute to κ_{xy}, which is consistent with speculations on the nature of the neutral excitation responsible for the sizable thermal Hall conductivity seen in the cuprates.[GLB19]

There are strong constraints and unique properties associated with the DM vectors that are generated by triplet density waves. Because triplet density wave states break spin-rotational invariance the associated Goldstone boson excitations will destroy the two dimensional triplet density wave order at finite temperatures. However, we find that when the underlying band structure is sufficiently topologically nontrivial insofar as it hosts a nonzero spin Hall conductance, and an external magnetic field is turned on, the triplet density wave induced DM vectors are energetically stable. Furthermore, these DM vectors are pinned to be collinear with the magnetic field, regardless of its direction, and the DM interaction will have the same symmetry as the form factor of the triplet density wave.

In the following we derive the DM coefficients induced by triplet density waves and investigate the effects they have on the physics of the underlying spin textures of the lattice. We find that for a ferromagnetic background, the ground state remains perfectly collinear below some critical strength of the density wave; above the critical strength, the ground state acquires a nonzero canting angle, and we show that quantum fluctuations correct the classically-predicted threshold for nonzero canting angle. Furthermore, we quantify the dependence of the spin stiffness on the strength of the density wave. For an antiferromagnetic background we find that below a critical density wave strength, perfect Neel order survives in the classical ground state, and above the critical strength the classical ground state acquires

a nonzero canting angle. We compute the spin-wave spectrum and find that for a particular density wave strength, the number of zero modes doubles, indicating a possible multicritical point.

4.2 The Effective Magnetic Hamiltonian

For any type of mixed triplet-singlet density wave condensation the mean-field Hamiltonian can be written in the suggestive manner

$$H = \sum_{ij} c^\dagger_{i\alpha}(t_{ij}\boldsymbol{\delta}_{\alpha,\beta} + i\boldsymbol{\lambda}_{ij}\cdot\boldsymbol{\sigma})c_{j\beta} \tag{4.7}$$

where all singlet density wave terms are absorbed into the definition of t_{ij}, and $\boldsymbol{\lambda}_{ij}$ are the triplet density wave terms which couple to $\boldsymbol{\sigma}$. It can be shown[KKM10] that this $\boldsymbol{\lambda}_{ij}$ induces a DM interaction in the underlying spin structure whose coefficients are given by

$$\mathbf{D}_{ij} = \boldsymbol{\lambda}_{ij}\mathrm{Tr}_{\,\sigma} N_{ji}, \tag{4.8}$$

where $N_{ji} \equiv \langle c^\dagger_i c_j\rangle = -\frac{1}{\pi}\int_{-\infty}^{E_F} \mathrm{Im}\, G_{ji}(E)dE$, $G_{ji}(E)$ is the Green function defined by H, and E_F is the Fermi energy. An expansion of $G_{ji}(E) = f(E)t_{ji}/t + g(E)\boldsymbol{\lambda}_{ji}\cdot\boldsymbol{\sigma}/t + \mathcal{O}(\lambda^2/t)$ reveals that the leading contribution to $G_{ji}(E)$ should have the same symmetry as t_{ji} under rotations. In this work we consider a specific example of Eq. (4.1), written in real space as

$$H_{\mathrm{DDW}} = H_0 + H_t + H_s \tag{4.9}$$

where H_0 is the tight binding Hamiltonian of the underlying crystal lattice which is some union of all square planar lattices which host the triplet-singlet DDW. For this triplet-singlet DDW case, because $\boldsymbol{\lambda}_{ij}$ only connects nearest neighbors, t_{ji} is simply the tight-binding kinetic energy coefficient which we will assume to transform trivially under rotation–thus we write

$$\mathbf{D}_{ij} = \alpha\boldsymbol{\lambda}_{ij} \tag{4.10}$$

for some constant α. Because we will allow the density wave strength to be a tunable parameter we will henceforth absorb α, and all other constant numerical prefactors into the

definition of W_0. The DM coefficients for the triplet $d_{x^2-y^2}$-density wave therefore become

$$\begin{aligned} D^{\mathbf{N}}_{i,i\pm a\hat{x}} &= (-1)^{i_x+i_y} W_0 \\ D^{\mathbf{N}}_{i,i\pm a\hat{y}} &= -(-1)^{i_x+i_y} W_0, \end{aligned} \tag{4.11}$$

where $i = i_x + i_y$, and the superscript $\mathbf{N}$ denotes that the DM vector points along the $\mathbf{N}$ direction. We stress that the method implemented here can be applied, in general, to triplet density waves in any angular momentum channel. The direction of the DM vector is along the triplet quantization axis, and the form factor associated with the triplet density wave dictates the symmetry of the DM vector on the lattice.

For a density wave-induced DM interaction to not be disordered by Goldstone modes at finite temperatures there must be some mechanism which externally stabilizes the triplet density wave's quantization axis, i.e. the direction of $\mathbf{N}$. It was recently shown[LL19] that the direction of $\mathbf{N}$ for the triplet-singlet DDW can be stabilized by the bulk orbital magnetization's coupling to the magnetic field. Explicitly, a magnetic field induces a bulk orbital magnetization, M, which is given by[CTV06]

$$M = -\sum_{\alpha=\mathbf{N}\cdot\boldsymbol{\sigma}=\pm 1} \frac{e}{hc} C_\alpha \Delta E_{Z,\alpha}, \tag{4.12}$$

where C_α is the Chern number of the band of spin α, e is the electron charge h is Planck's constant, c is the speed of light, and $\Delta E_{Z,\alpha}$ is the Zeeman splitting

$$\Delta E_{Z,\alpha} = -\alpha \mu_B \mathrm{sgn}(W_0) \mathbf{N} \cdot \mathbf{B}, \tag{4.13}$$

where μ_B is the Bohr magneton. For the case of the triplet-singlet DDW the resulting energy density due to the orbital magnetization-magnetic field is[LL19]

$$\Delta \mathcal{E}_{\text{Zeeman}} = -\frac{\mu_B B^2}{\pi c} \mathrm{sgn}(W_0 \Delta_0)(\mathbf{N} \cdot \hat{\mathbf{B}}), \tag{4.14}$$

which implies that it is energetically most favorable for $W_0 \Delta_0 \mathbf{N} \parallel \mathbf{B}$. Thus, for $\Delta_0 > 0$, $\mathbf{B} \neq 0$, Eq. 4.11 necessarily becomes

$$\begin{aligned} D^{\mathbf{B}}_{i,i\pm a\hat{x}} &= (-1)^{i_x+i_y} |W_0| \\ D^{\mathbf{B}}_{i,i\pm a\hat{y}} &= -(-1)^{i_x+i_y} |W_0|. \end{aligned} \tag{4.15}$$

From this argument alone we see that stable density wave-induced DM interactions can only arise from topological density waves with nonvanishing spin Hall conductance–that is, given $\Delta E_{Z,+1} = -\Delta E_{Z,-1}$, stability is only guaranteed if $C_{+1} = -C_{-1}$. Furthermore, because density wave-induced DM vectors must be collinear with the magnetic field, they will transform like the magnetic field under rotations and time-reversal. This immediately implies that the corresponding magnons in the problem will have no contribution to any thermal Hall effect because of the spin rotation and time-reversal symmetry considerations, namely[SCS19]

$$\begin{aligned} \kappa_{xy}[J, \mathbf{D}_{ij}, \mathbf{B}] &= \kappa_{xy}[J, R_{\boldsymbol{\phi}}\hat{\mathbf{B}}D_{ij}, R_{\boldsymbol{\phi}}\mathbf{B}] \\ \kappa_{xy}[J, \mathbf{D}_{ij}, \mathbf{B}] &= -\kappa_{xy}[J, -\hat{\mathbf{B}}D_{ij}, -\mathbf{B}] \end{aligned} \tag{4.16}$$

where $R_{\boldsymbol{\phi}}$ is the vector representation of spin rotation by some angle ϕ about the axis defined by $\hat{\boldsymbol{\phi}}$. Rotating the system about an angle π about an axis perpendicular to $\hat{\mathbf{B}}$ maps $R_{\boldsymbol{\phi}}\hat{\mathbf{B}}$ to $-\hat{\mathbf{B}}$ and hence $\kappa_{xy} = -\kappa_{xy} = 0$. The bulk magnetization (Eq. 4.12) would, in principle, produce a small ferromagnetic-like signal detectable in polar Kerr measurements so long as the external magnetic field is not exactly zero for weak disorder at small enough temperatures. More detailed calculations involving interlayer coupling, the inclusion of magnetic impurities, and nonzero temperatures should be considered in future work to quantitatively compare this triplet-singlet DDW bulk magnetization signal to the polar Kerr rotation data previously gathered[XSD08]. Furthermore, it is an interesting question to ask how the Goldstone modes would disorder the DM vectors and study their effects on the underlying magnetization in the absence of an external magnetic field or for triplet density wave states with vanishing spin Hall conductances.

We now study the effect of this dynamically generated DM interaction on the isotropic Heisenberg ferromagnet and antiferromagnet. Namely, we consider

$$H = J\sum_{i,j} \mathbf{S}_i \cdot \mathbf{S}_j + \sum_{i,j} \mathbf{D}_{ij} \cdot (\mathbf{S}_i \times \mathbf{S}_j) - \mathbf{B} \cdot \sum_i \mathbf{S}_i, \tag{4.17}$$

where J is the spin exchange, and the DM interaction includes the contribution from the density wave.

4.3 The Noncollinear Ferromagnet

It has previously been shown[KK03] via a one-loop renormalization group analysis of the extended U-V-J model that triplet density wave condensation is energetically favorable for a range of interaction strengths, given $J/U < 0$. Thus we begin by considering the uniform ferromagnetic case $J < 0$. Taking $\mathbf{B} = B\hat{z}$ the symmetric exchange term favors mean-field states of the form

$$\langle \bar{\mathbf{S}}_i \rangle = n_z \hat{z}, \tag{4.18}$$

and the antisymmetric exchange favors mean-field states of the form

$$\begin{aligned} \langle \tilde{\mathbf{S}}_i \rangle &= \xi_x(\mathbf{r}_{i_x,i_y})\hat{x} + \xi_y(\mathbf{r}_{i_x,i_y})\hat{y}, \\ \xi_x(\mathbf{r}_i) &= \xi_0 \frac{[(-1)^{i_x} + (-1)^{i_y}]}{2} \\ \xi_y(\mathbf{r}_i) &= \xi_0 \frac{[(-1)^{i_x} - (-1)^{i_y}]}{2}. \end{aligned} \tag{4.19}$$

Thus, the mean-field state which occurs in the presence of both types of exchange is

$$S\langle \mathbf{n}_i \rangle = \langle \bar{\mathbf{S}}_{i_x,i_y} \rangle + \langle \tilde{\mathbf{S}}_{i_x,i_y} \rangle. \tag{4.20}$$

The mean-field energy per site in this case is

$$\begin{aligned} \frac{E_0}{N} = &-|J|S^2 z \cos^2(\theta)/2 - 2S^2|W_0|\sin^2(\theta) \\ &- BS\cos(\theta), \end{aligned} \tag{4.21}$$

where N is the number of lattice sites, $z = 4$ (6) in two (three) dimensions, and θ is defined as the angle between $\langle \bar{\mathbf{S}}_{i_x,i_y} \rangle$ and $\langle \tilde{\mathbf{S}}_{i_x,i_y} \rangle$. For the square lattice case, with B small, the ground state is minimized about $\theta = 0$ for all $2W_0 < z|J|/2$, whereas the ground state is minimized at $\theta = \pi/2$ for $2W_0 > z|J|/2$.

To gain insight into the quantum behavior of this spin Hamiltonian we focus on the two dimensional case and expand our spin operators about the mean-field ground state[Fis04, HF09]

$$\mathbf{S}_i = a_i \langle \mathbf{n}_i \rangle + \mathbf{t}_i \tag{4.22}$$

so that we can perform the appropriate Holstein-Primakoff substitution. The amplitudinal reduction along the mean-field state given as

$$a_i = S - b_i^\dagger b_i, \tag{4.23}$$

and, to leading order in boson density operators, the transverse fluctuation operator $\mathbf{t}_i$ is given by

$$\mathbf{t}_i = t_i^{x'}\hat{x}_i' + t_i^{y'}\hat{y}_i', \tag{4.24}$$

with

$$\begin{aligned} t_i^{x'} &= \sqrt{\frac{S}{2}}(b_i^\dagger + b_i) \\ t_i^{y'} &= i\sqrt{\frac{S}{2}}(b_i^\dagger - b_i) \end{aligned} \tag{4.25}$$

where the primed coordinates are defined such that $\hat{x}_i' \times \hat{y}_i' = \langle \mathbf{n}_i \rangle$. Upon substitution of these operators into Eq. (16) the Hamiltonian can be written in real space as

$$H = E_0 + H_0 + H', \tag{4.26}$$

where the classical mean field energy E_0 is defined in Eq. (20), H_0 is

$$\begin{aligned} H_0 = \sum_i \mu b_i^\dagger b_i + \sum_{\langle i,j \rangle} [&\bar{Z}_\theta g(j) b_i^\dagger b_j + \tilde{Z}_\theta g(j) b_i^\dagger b_j^\dagger \\ &+ iJS\cos(\theta)(-1)^{i_x+i_y} b_i b_j^\dagger + \text{h.c.}], \end{aligned} \tag{4.27}$$

with $g(j) = +1$ for $j = i + \hat{x}$, and $g(j) = -1$ for $j = i + \hat{y}$, and the coefficients are defined as

$$\begin{aligned} \bar{Z}_\theta &\equiv \frac{JS}{2}\sin^2(\theta) + \frac{W_0 S}{2}(\cos^2(\theta) + 1) \\ \tilde{Z}_\theta &\equiv \frac{JS}{2}\sin^2(\theta) + \frac{W_0 S}{2}(\cos^2(\theta) - 1) \\ \mu &\equiv 4J\cos^2(\theta) + 4W_0\sin^2(\theta) + B\cos(\theta), \end{aligned} \tag{4.28}$$

and H' is

$$H' = \sum_i (-1)^{i_x} A_\theta (b_i^\dagger + b_i), \tag{4.29}$$

where

$$A_\theta = \sin(\theta)\left[\sqrt{\frac{S}{2}}B - \left((2S)^{3/2} + 4SW_0\right)\cos(\theta)\right]. \tag{4.30}$$

Terms linear in boson creation and annihilation operators imply spin-wave creation and annihilation from the ground state. Thus, assuming that the system is in its ground state, it is typically argued that this coefficient A_θ must vanish at each point i on the lattice. There exist two unique solutions for vanishing A_θ: The perfectly ferromagnetic case of $\theta = 0$, and

$$|\theta| = \cos^{-1}\left[\frac{B}{4SJ + 4\sqrt{2S}W_0}\right] \tag{4.31}$$

which is a modified version of the flopped magnetic ground state that occurs at the classical mean-field level when $W_0 > J$.

For our mean-field ansatz, if we were to restrict ourselves to only the case of vanishing A_θ the only stable ground state would occur when $\theta = 0$. This is inconsistent with our classical mean-field prediction of nonzero spin canting existing for some values of W_0. If we instead eliminate terms linear in bosonic creation and annihilation operators by performing the canonical transformation

$$\begin{aligned} b_i &= \tilde{b_i} - (-1)^{i_x} x \\ b_i^\dagger &= \tilde{b}_i^\dagger - (-1)^{i_x} x, \end{aligned} \tag{4.32}$$

where x_i is the C-number

$$x = \frac{-A_\theta}{4\bar{Z}_\theta + 4\tilde{Z}_\theta - \mu}, \tag{4.33}$$

the Hamiltonian then becomes

$$H = E_0 + N[x^2 + 2xA_\theta] + H_0' = E_0' + H_0', \tag{4.34}$$

where H_0' is identical to the Hamiltonian written in Eq. (27) but in terms of the transformed bosonic operators $\tilde{b}$. The modified ground state energy E_0' is minimized at $\theta = 0$ for all values of density wave strength up to a critical value $W_0^* \approx 0.75$ where B is taken small and so the linear bosonic terms and corrections to the ground state are absent. Tuning past W_0^*, however, the ground state energy is minimized about nonzero θ canted away the z-axis. We plot this corrected ground state canting angle for fixed B as a function of W_0 in Fig. 4.2, and for fixed W_0 as a function of B in Fig. 4.3. We see in Fig. 4.2 that canting away from the z-axis occurs well before the classically predicted threshold of $W_0 = J$, and that the change

in ground state spin orientation is not discontinuous as predicted by the classical case of Eq. 20.

Upon Fourier transformation the magnon Hamiltonian H_0' can be written in the Nambu basis as

$$\sum_k \frac{1}{2}\psi_k^\dagger \mathcal{H}_k \psi_k \tag{4.35}$$

where $\psi_k^\dagger = (\tilde{b}_k^\dagger, \tilde{b}_{-k}, \tilde{b}_{k+Q}^\dagger, \tilde{b}_{-k+Q})$, and

$$\mathcal{H}_k = \begin{pmatrix} \bar{Z}_{\theta,k} + \mu & 2\tilde{Z}_{\theta,k} & 2iJ_k\cos(\theta) & 0 \\ 0 & \bar{Z}_{\theta,k} + \mu & 0 & -2iJ_k\cos(\theta) \\ 0 & 0 & -\bar{Z}_{\theta,k} + \mu & -2\tilde{Z}_{\theta,k} \\ 0 & 0 & 0 & -\bar{Z}_{\theta,k} + \mu \end{pmatrix} + \text{h.c.} \tag{4.36}$$

To diagonalize the 4×4 matrix $\mathcal{H}_k$ we must find the appropriate paraunitary matrix, T_k, which preserves the bosonic commutation relations among the eigenvectors[SMM13]. First, we numerically compute the Cholensky decomposition of $\mathcal{H}_k$, solving for $\mathcal{H}_k = K_k^\dagger K_k$, where K_k is an upper triangular matrix. Next, we define $W_k = K_k \rho_3 K_k^\dagger$, where $\rho_3 = \sigma_3 \otimes \mathbb{I}_2$. We then obtain the unitary matrix which diagonalizes W_k, producing

$$U_k^\dagger W_k U_k = \text{diag}(\vec{E}_k, -\vec{E}_{-k}), \tag{4.37}$$

where E_k are the energy eigenvalues. We use this unitary matrix to define the matrix T_k

$$T_k = K_k^{-1} U_k \text{diag}(\overrightarrow{\sqrt{E}_k}, \overrightarrow{\sqrt{E}_{-k}}) \tag{4.38}$$

which satisfies

$$T_k^\dagger H_k T_k = \text{diag}(\vec{E}_k, \vec{E}_{-k}) \tag{4.39}$$

and is also para-unitary ($T_k^\dagger \rho_3 T_k = \rho_3$). The dispersion E_{k_x} with $k_y = 0$ is plotted for some representative values of B, W_0 in Figs. 4.4 and 4.5. The dispersion along k_y with $k_x = 0$ is identical. Importantly, $E_k > 0$ for all k which implies that E_0' is the true groundstate of our Hamiltonian at sufficiently low temperatures. For the long wavelength limit the spin-wave stiffness is given via $E_k \approx \mu + \rho_s k^2$ where μ is the energy gap induced by the magnetic field

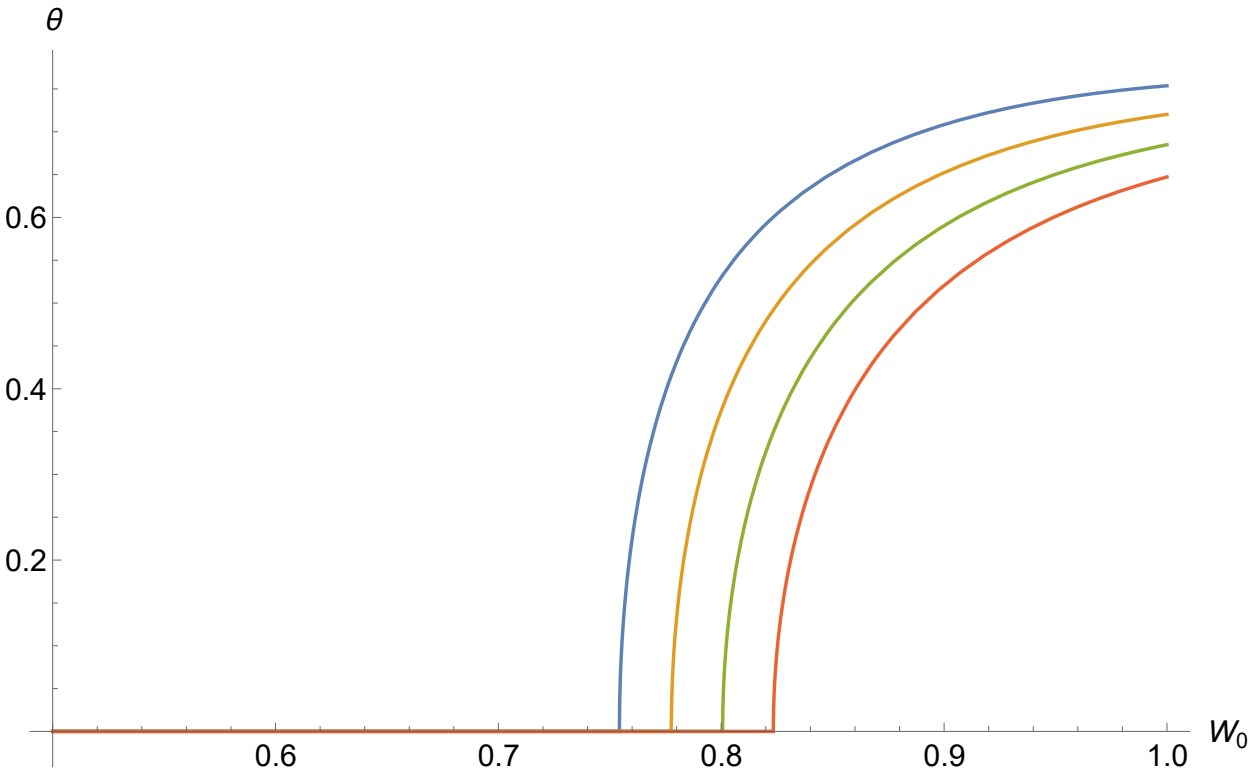

Figure 4.2: The ground state canting angle θ as a function of W_0 (listed in units of J). The blue, orange, green, red curves correspond to $B = 0.05J$, $B = 0.1J$, $B = 0.15J$, and $B = 0.2J$ respectively.

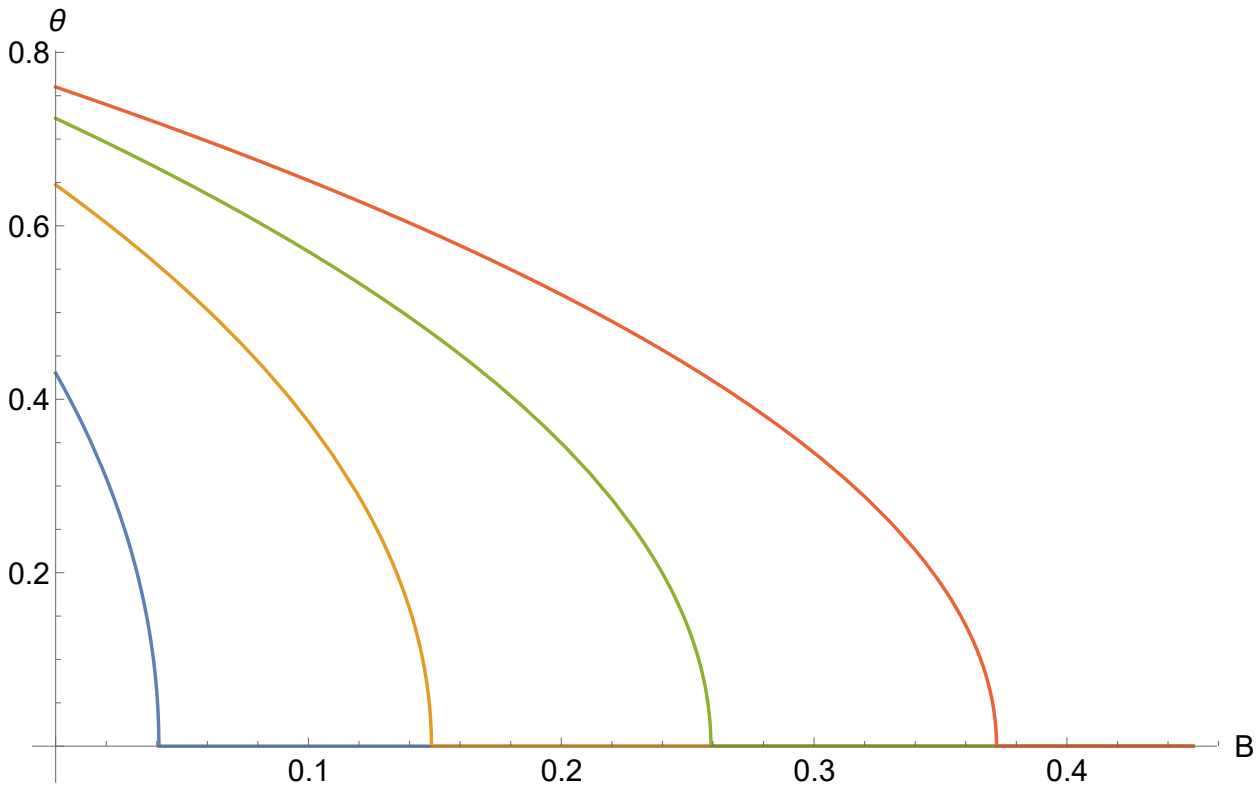

Figure 4.3: The ground state canting angle θ as a function of B (listed in units of J). The blue, orange, green, red curves correspond to $W_0 = 0.75J$, $W_0 = 0.8J$, $W_0 = 0.85J$, and $W_0 = 0.9J$ respectively.

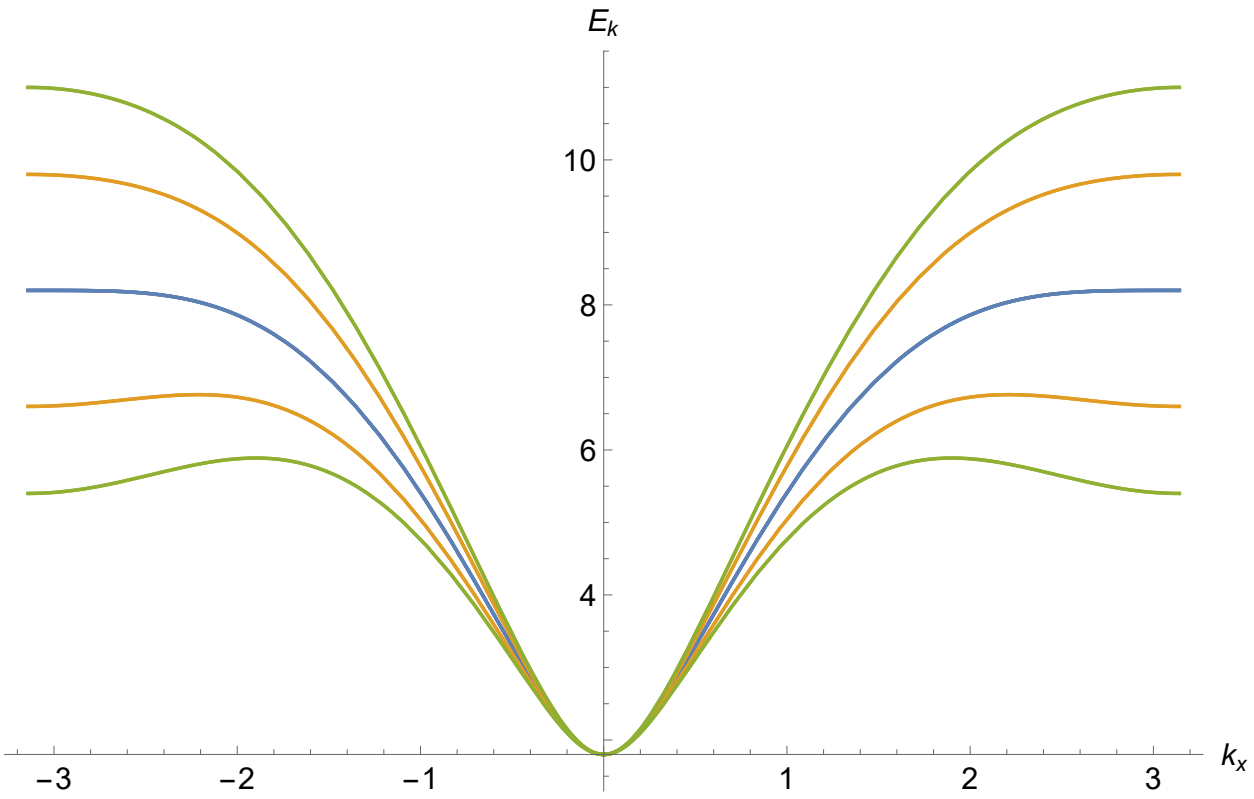

Figure 4.4: Magnon dispersion E_{k_x} in units of J for various values of density wave strength with $B = 0.1J$. The blue, orange, and green curves correspond to $W_0 = 0$, $W_0 = 0.4J$, and $W_0 = 0.7J$ respectively, all below W_0^*. In this regime, increasing W_0 does not change the minimum energy.

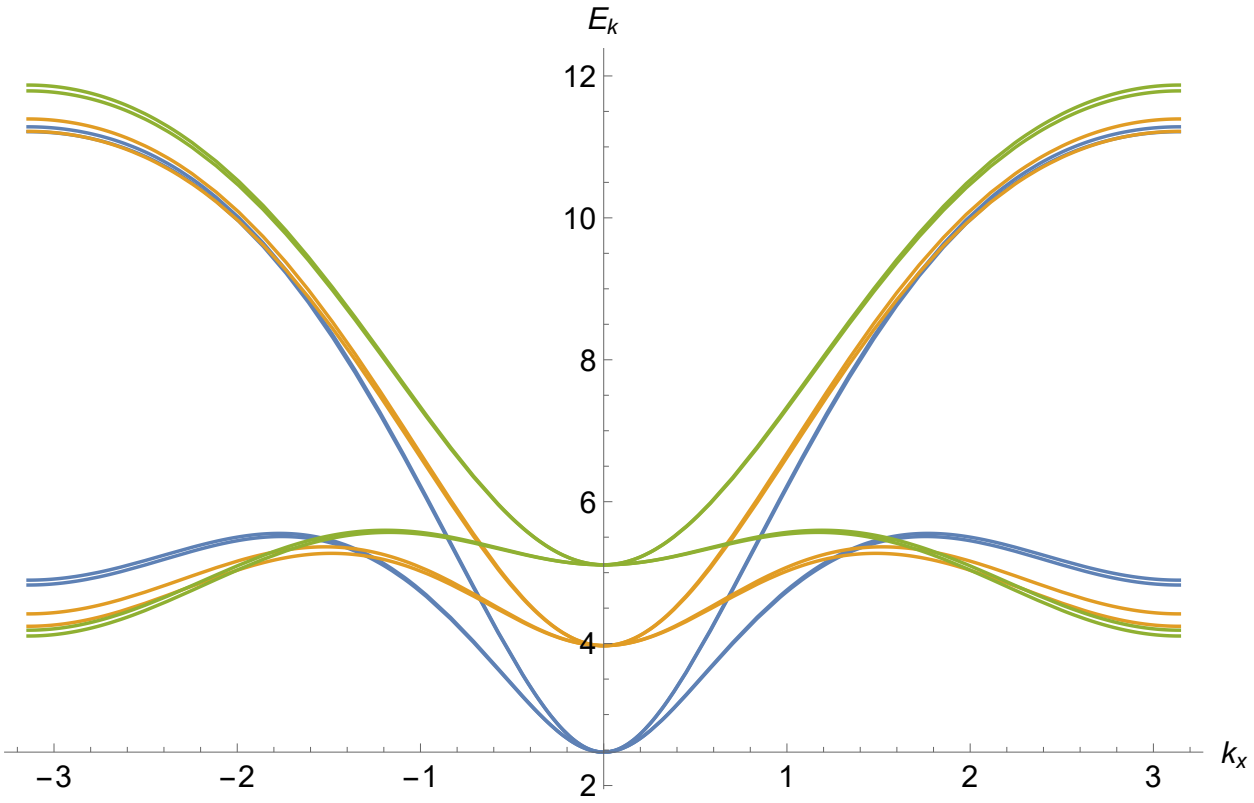

Figure 4.5: Magnon dispersion E_{k_x} in units of J for various values of density wave strength with $B = 0.1J$. The blue, orange, and green curves correspond to $W_0 = 0.79J$, $W_0 = 0.85J$, and $W_0 = 0.95J$ respectively, all above W_0^*. In this regime, increasing W_0 increases the minimum energy.

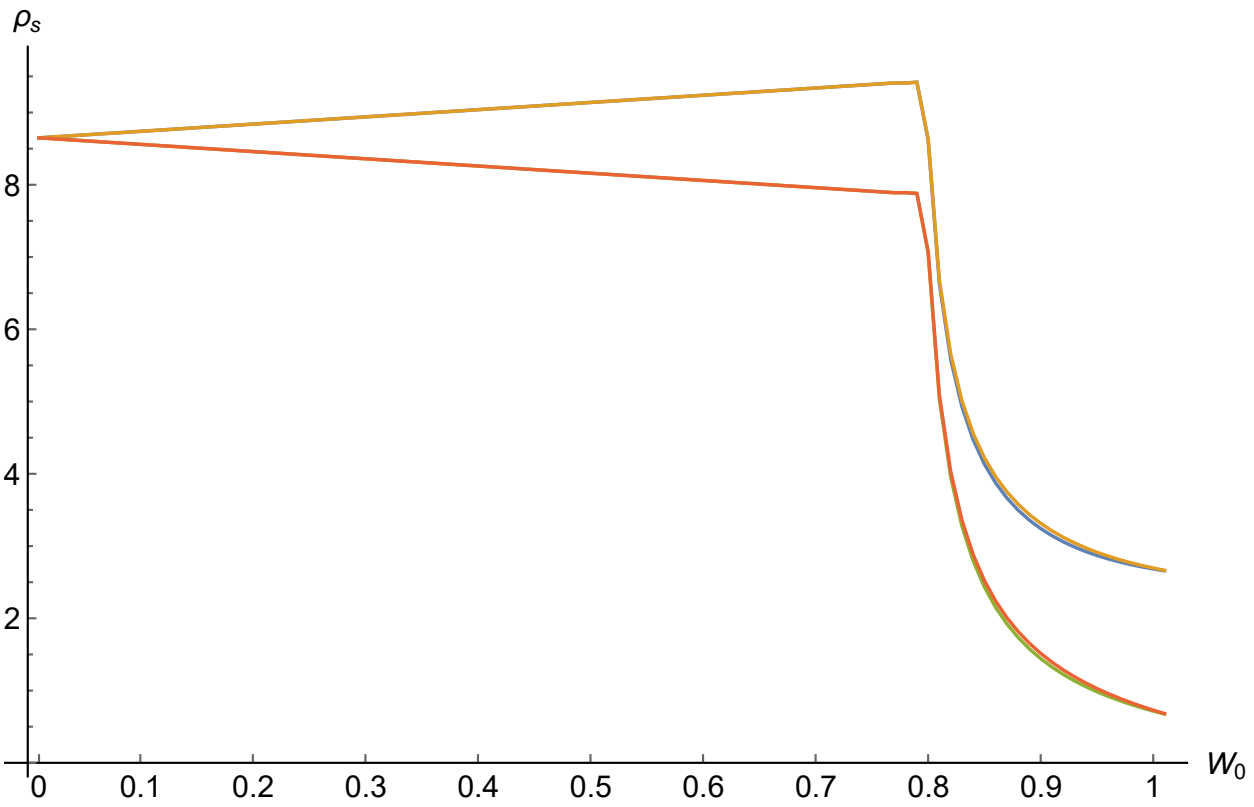

Figure 4.6: Dimensionless spin-wave stiffness of the canted ferromagnet as a function of W_0 (listed in units of J). The two curves correspond to the two different bands.

and spin canting. Using a parabolic fitting program we plot the dimensionless spin-wave stiffness versus density wave strength in Fig. 4.6. To good approximation we find that (setting the lattice spacing to unity) $\rho_s = \rho_s^0 \pm W_0$ for density wave strengths up to the critical value W_0^*. Tuning past W_0^* the spin-wave stiffness contribution from $k = 0$ behaves asymptotically as $\rho_s = K_1 \csc\left[\frac{W_0 - W_0^*}{K_2}\right]$ for some constants K_1 and K_2 up to $W_0 = J$.

4.4 The Noncollinear Antiferromagnet

4.4.1 Mean-Field Theory

Taking $\mathbf{B} = B_z\hat{z}$ (note the change in notation for the magnetic field strength) the DM matrix for LSCO can be written as $\mathbf{D}_i = (-1)^{i_x+i_y}\mathbf{D}$, where

$$\mathbf{D} = \begin{pmatrix} \sqrt{2}D\cos\theta_d & \sqrt{2}D\sin\theta_d & W_0 \\ -\sqrt{2}D\sin\theta_d & -\sqrt{2}D\cos\theta_d & -W_0 \\ 0 & 0 & 0 \end{pmatrix}. \tag{4.40}$$

The x and y spin direction entries are due to the buckling of the oxygen atoms out of the copper oxide plane and induce a weak net ferromagnetic moment out of the copper oxide plane.[CTF89, CRZ91, TA94] For our investigation we will set $D = 0$ and only consider the effect of the density wave induced terms. We first investigate the mean-field ground state spin texture in the presence of the triplet density wave in the following. Mean-field states of the form

$$\begin{aligned} \langle\tilde{\mathbf{S}}_{m,n}\rangle &= \xi_x(\mathbf{r}_{m,n})\hat{x} + \xi_y(\mathbf{r}_{m,n})\hat{y} \\ \xi_x(\mathbf{r}_{m,n}) &= \xi_0\cos(\pi n)\cos^2\left(\frac{\pi}{2}(m+n)\right) \\ \xi_y(\mathbf{r}_{m,n}) &= \xi_0\cos(\pi m)\sin^2\left(\frac{\pi}{2}(m+n)\right) \end{aligned} \tag{4.41}$$

are the most energetically favorable for the antisymmetric exchange interaction as was the case for the ferromagnetic background. On the other hand, the symmetric exchange term favors mean-field states of the form

$$\langle\bar{\mathbf{S}}_{m,n}\rangle = n_x(-1)^{m+n}\hat{x} + n_y(-1)^{m+n}\hat{y}, \tag{4.42}$$

where we have assumed an in-plane antiferromagnetic order parameter due to the spin flopping that occurs when the magnetic field $\mathbf{B} = B_z\hat{z}$ is turned on. In the following we take the somewhat special case $n_x = n_y = n_a/\sqrt{2}$, and study the mean-field ground state

$$\langle\mathbf{S}_{m,n}\rangle = \langle\bar{\mathbf{S}}_{m,n}\rangle + \langle\tilde{\mathbf{S}}_{m,n}\rangle \tag{4.43}$$

which occurs in the presence of both types of exchange. Upon normalization the local mean-field energy is

$$\begin{aligned}\langle H_{mn}\rangle = &-(2Jn_a^2 + 2W_0\xi_0^2)\left[\frac{1}{N_{m,n}^2} + \frac{1}{\sqrt{\xi_0^4 + n_a^4}}\right] \\ &- 2\sqrt{2}(J + W_0)\frac{\xi_0 n_a(-1)^n}{N_{m,n}^2}\end{aligned} \tag{4.44}$$

where $N_{m,n}^2 = \xi_0^2 + n_a^2 + \sqrt{2}n_a\xi_0\cos(\pi n)$ is the square of the normalization and we have summed only over the nearest neighbor terms. To study the canting angle induced by the DMI we define $(n_a/\sqrt{2} + \xi_x(\mathbf{r}_{m,n}))/N_{m,n} = \cos\theta_c(\mathbf{r}_{m,n})$ and $(n_a/\sqrt{2} + \xi_y(\mathbf{r}_{m,n}))/N_{m,n} = \sin\theta_c(\mathbf{r}_{m,n})$. For the $m+n$ odd sublattice this local mean-field energy $\langle H_{mn}^{\text{odd}}\rangle$ can be written in terms of the angle $\theta_c(\mathbf{r}_{m+n=\text{odd}}) = \theta_o$ as

$$\begin{aligned}\langle H_{mn}^o\rangle = &-4(J + W_0)\cos\theta_0[\sin\theta_o - \cos\theta_o] \\ &+ \frac{2J\cos^2\theta_o - 2W_0(1 - 2\cos\theta_o\sin\theta_o)}{\sqrt{(1 - 2\sin\theta_o\cos\theta_o)^2 + (2\cos^2\theta_o)^2}} \\ &- 2\left[2J\cos^2\theta_o + W_0(1 - 2\sin\theta_o\cos\theta_o)\right].\end{aligned} \tag{4.45}$$

Now we notice that θ_o and $\theta_c(\mathbf{r}_{m+n=\text{even}}) = \theta_e$ are related via trigonometric functions in a simple way: $\sin^2\theta_o = \cos^2\theta_e$, $\cos^2\theta_o = \sin^2\theta_e$, and $\sin\theta_o\cos\theta_o = \sin\theta_e\cos\theta_e$. Thus

$$\begin{aligned}\langle H_{mn}^{\text{even}}\rangle = &-2[(J + W_0)[2\sin\theta_o\cos\theta_o - 2\sin^2\theta_o] \\ &+ \frac{2J\sin^2\theta_o - 2W_0(1 - 2\cos\theta_o\sin\theta_o)}{\sqrt{(1 - 2\sin\theta_o\cos\theta_o)^2 + (2\sin^2\theta_o)^2}}] \\ &- 2[2J\sin^2\theta_o + W_0(1 - 2\sin\theta_o\cos\theta_o)]\end{aligned} \tag{4.46}$$

We sum the local mean-field energy over the two sublattices $m + n$=even and $m + n$=odd, and numerically minimize the total ground state energy in terms of θ_o. We find that for values of the density wave strength $W_0 < 0.848J$, $\theta_o = 5\pi/4$ is the only stable minimum–i.e. the system is in the perfectly antiferromagnetic state. By tuning past the critical value of $W_0^* \approx 0.848J$, however, the energy is minimized about $\theta_o = 5\pi/4 \pm \theta'$, where θ' is some nonzero canting angle with respect to the $x = y$ axis. For example, at $W_0 = 0.9J$ we find that $\theta' \approx 0.29$ radians. We plot the the dependence of the canting angle on W_0 in Fig. 4.9 and the ground state spin texture in Figs. 4.7 and 4.8.

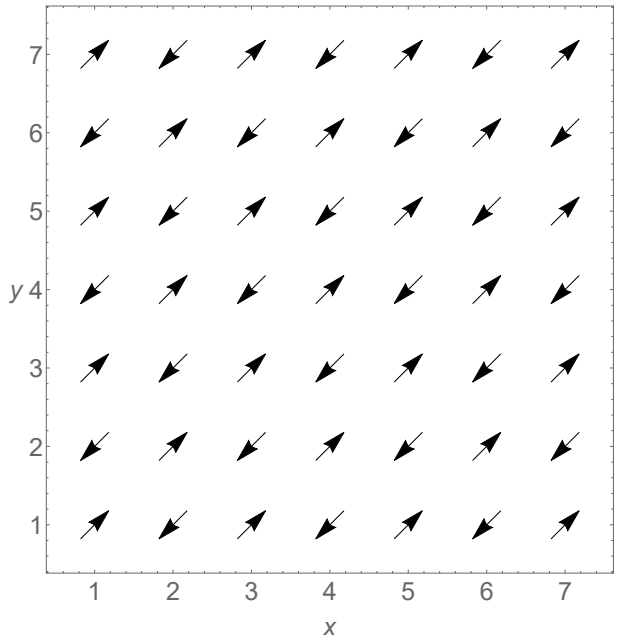

Figure 4.7: Classical ground state spin texture for the antiferromagnet in real space for $W_0 < 0.848J$. The x and y axes are in units of the lattice spacing.

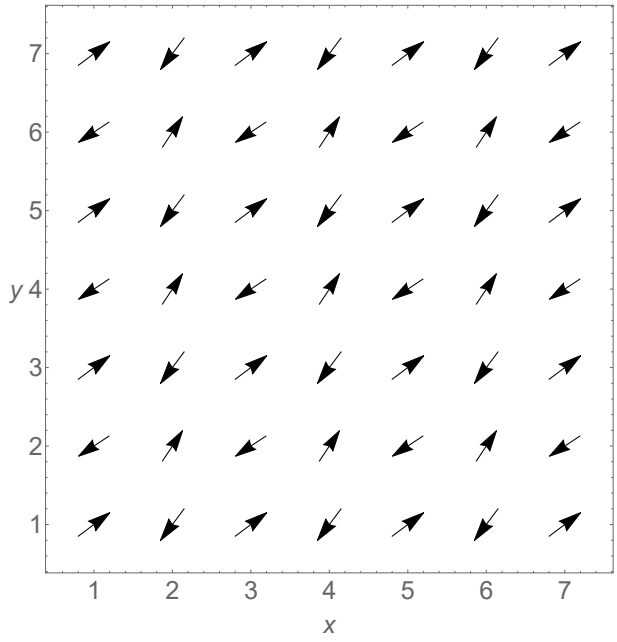

Figure 4.8: Classical ground state spin texture for the antiferromagnet in real space for $W_0 = 0.9J$. The x and y axes are in units of the lattice spacing.

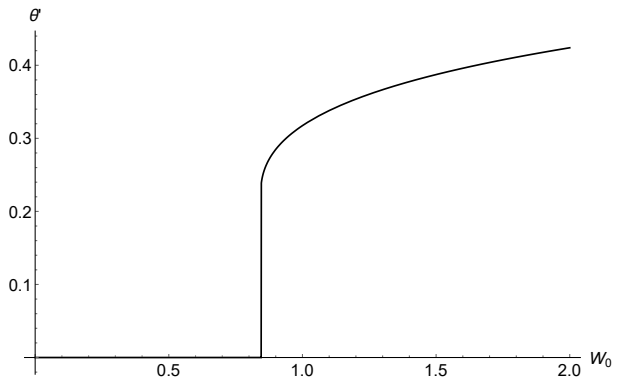

Figure 4.9: The absolute value of the mean-field antiferromagnetic ground state canting angle θ' as a function of W_0 (listed here in units of J).

4.4.2 Schwinger Boson Mean-Field Theory

To gain insight into the antiferromagnetic spin-wave excitations we utilize Schwinger boson mean-field theory (SBMFT) as for this problem it is considerably more computationally convenient than the Holstein-Primakoff approach. In SBMFT the spin operator $\mathbf{S}_i$ is written in terms of Schwinger bosons as

$$\mathbf{S}_i = \frac{1}{2}\sum_{\sigma,\sigma'} b^\dagger_{i,\sigma}\boldsymbol{\sigma}_{\sigma,\sigma'}b_{i,\sigma'}, \tag{4.47}$$

where b_i, $b_i^\dagger$, satisfy bosonic commutation relations. Insisting that $\sum_\sigma b^\dagger_{i,\sigma}b_{i,\sigma} = 2S$ closes the algebra, and ensures $\mathbf{S}_i^2 = S(S+1)$. In the manipulations below, we employ the looser constraint that this holds only on average: $\langle\hat{n}\rangle = 2S$.

We wish express our Hamiltonian Eq. (18) in terms of these Schwinger bosons. To do so we define the operators

$$\begin{aligned}
\hat{A}_{i,j} &= \frac{1}{2}\sum_{\sigma,\sigma'} b_{i,\sigma}(i\sigma_2)_{\sigma,\sigma'}b_{j,\sigma'} \\
\hat{B}_{i,j} &= \frac{1}{2}\sum_{\sigma} b_{i,\sigma}b^\dagger_{j,\sigma} \\
\hat{C}^\dagger_{i,j} &= \frac{1}{2}\sum_{\sigma,\sigma'} b^\dagger_{i,\sigma}(i\mathbf{d}_{i,j}\cdot\boldsymbol{\sigma})_{\sigma,\sigma'}b_{j,\sigma'} \\
\hat{D}_{i,j} &= \frac{1}{2}\sum_{\sigma,\sigma'} b_{i,\sigma}(\sigma_2\mathbf{d}_{i,j}\cdot\boldsymbol{\sigma})_{\sigma,\sigma'}b_{j,\sigma'},
\end{aligned} \tag{4.48}$$

which satisfy $\hat{A}_{i,j} = -\hat{A}_{j,i}$, $\hat{B}^{\dagger}_{i,j} = \hat{B}_{j,i}$, $\hat{C}^{\dagger}_{i,j} = \hat{C}_{j,i}$, and $\hat{D}_{i,j} = -\hat{D}_{j,i}$. Then, using the following identities (note the change in notation from $\mathbf{D}_{i,j}$ in Eq. (18) to $\mathbf{d}_{i,j}$),

$$\begin{aligned} \mathbf{S}_i \cdot \mathbf{S}_j &=: \hat{B}^{\dagger}_{i,j}\hat{B}_{i,j} : -\hat{A}^{\dagger}_{i,j}\hat{A}_{i,j} \\ \mathbf{d}_{i,j} \cdot (\mathbf{S}_i \times \mathbf{S}_j) &= \frac{1}{2}(: \hat{B}^{\dagger}_{i,j}\hat{C}_{i,j} + \hat{C}^{\dagger}_{i,j}\hat{B}_{i,j} : \\ &\qquad + \hat{A}^{\dagger}_{i,j}\hat{D}_{i,j} + \hat{D}^{\dagger}_{i,j}\hat{A}_{i,j}) \end{aligned} \tag{4.49}$$

our Hamiltonian becomes

$$\begin{aligned} H = J \sum_{\langle i,j \rangle} &(\hat{B}^{\dagger}_{i,j}\hat{B}_{i,j} - \hat{A}^{\dagger}_{i,j}\hat{A}_{i,j} - \frac{1}{4}\hat{n}_i) \\ &+ \frac{1}{2}\sum_{\langle i,j \rangle}(\hat{B}^{\dagger}_{j,i}\hat{C}_{i,j} + \hat{C}^{\dagger}_{i,j}\hat{B}_{i,j} \\ &+ \hat{A}^{\dagger}_{i,j}\hat{D}_{i,j} + \hat{D}^{\dagger}_{i,j}\hat{A}_{i,j}) \\ &- B_z\hat{z} \cdot \sum_i \mathbf{S}_i + \sum_i \lambda(\hat{n}_i - 2S). \end{aligned} \tag{4.50}$$

The final term is a Lagrange multiplier enforcing the spin constraint.

Now we enact a mean-field decoupling on the operators $\hat{A}_{i,j}$ and $\hat{B}_{i,j}$, replacing them with their average values, $A_{i,j}$ and $B_{i,j}$. The choice for the form of $A_{i,j}$ and $B_{i,j}$ defines our mean-field ansatz. The ansatz must be such that the symmetries of the lattice, as well as the constraints on $\hat{A}_{i,j}$ and $\hat{B}_{i,j}$, are respected. Furthermore, the choice of ansatz defines the phase of the resulting spin liquid.

Because $A_{i,j}$ and $B_{i,j}$ are not physical quantities, and are therefore dependent on the choice of gauge, we know two such ansätze (for example $A'_{i,j}$, $B'_{i,j}$ and $A_{i,j}$, $B_{i,j}$) correspond to the same physical system if they are linked by a gauge transformation. A symmetry X is then said to be obeyed by an ansatz if there exists some gauge transformation G_X such that the ansatz is left invariant under the operation $G_X X$. The set of operations $G \times X$ under which the ansatz remains invariant defines the projective symmetry group of this ansatz. Different ansätze can be distinguished by their corresponding gauge invariant physical quantities—in particular, the gauge invariant flux corresponding to a Wilson loop: e.g. $\Phi_1 = \mathrm{Arg}(A_{i,j}A^*_{j,k}A_{k,l}A^*_{l,i})$, where i, j, k, and l define a counter-clockwise loop about the elementary plaquette.

Using the machinery laid out in previous work[MLM13, YW16, SCS19], we determine the appropriate ansatz for our system. We insist that the lattice symmetries of the DM interaction are obeyed, and also that $A_{i,j} = -A_{j,i}$, and $B_{i,j} = B^*_{j,i}$. We are left with two choices of ansatz: a zero flux ansatz, and a π flux ansatz (defined by $\Phi_1 = 0, \pi$ respectively).

We use the zero flux ansatz, which is smoothly connected to the Neel state. Taking only nearest neighbor couplings to be nonzero, our ansatz is then

$$\begin{aligned} A_{\hat{x}} = -A_{-\hat{x}} = A \qquad A_{\hat{y}} = -A_{-\hat{y}} = -A \\ B_{\hat{x}} = -B_{-\hat{x}} = iB \qquad B_{\hat{y}} = -B_{-\hat{y}} = -iB \end{aligned} \tag{4.51}$$

To complete the mean-field procedure, we would next enforce self-consistency using the free energy, F:

$$\frac{\partial F}{\partial A_{i,j}} = \frac{\partial F}{\partial B_{i,j}} = \frac{\partial F}{\partial \lambda} = 0. \tag{4.52}$$

Here, however, we take A and B to be free parameters, with values limited by their upper bounds[MLM13]: $|A| \leq S + 1/2$, $|B| \leq 1/2$.

We can understand the physical correspondence of $\hat{A}_{i,j}$ and $\hat{B}_{i,j}$ through their effect as projection operators[MLM13]. Taking $\sum_\sigma b^\dagger_{i,\sigma} b_{i,\sigma} = 2S$, we may note that

$$\begin{aligned} \hat{A}^\dagger_{i,j}\hat{A}_{i,j} = \frac{1}{2}(\mathbf{S}_i \cdot \mathbf{S}_j - S^2) = \frac{1}{2}\hat{P}_s \\ :\hat{B}^\dagger_{i,j}\hat{B}_{i,j}: = \frac{1}{2}(\mathbf{S}_i \cdot \mathbf{S}_j + S^2) = \frac{1}{4}(\hat{P}_t - \hat{P}_s) \end{aligned} \tag{4.53}$$

where $\hat{P}_s$ projects onto the singlet state, and $\hat{P}_t$ projects onto the triplet state. Therefore $\hat{A}^\dagger_{i,j}\hat{A}_{i,j}$ yields the singlet part, while $:\hat{B}^\dagger_{i,j}\hat{B}_{i,j}:$ gives the ferromagnetic contribution.

We write our Hamiltonian in the form

$$H = \frac{1}{2}\Psi^\dagger M \Psi, \tag{4.54}$$

where $\Psi^\dagger = (b^\dagger_{k,\uparrow}, b^\dagger_{k+Q,\uparrow}, b_{-k,\downarrow}, b_{-k+Q,\downarrow})$, and

$$M = \begin{pmatrix} -\frac{B_z}{2} + 2BJS_1 - J + \lambda & -iBW_0S_2 & 2iAJS_1 & AW_0S_2 \\ iBW_0S_2 & -\frac{B_z}{2} - 2BJS_1 - J + \lambda & -AW_0S_2 & -2iAJS_1 \\ -2iAJS_1 & -AW_0S_2 & \frac{B_z}{2} - 2BJS_1 - J + \lambda & iBW_0S_2 \\ AW_0S_2 & 2iAJS_1 & -iBW_0S_2 & \frac{B_z}{2} + 2BJS_1 - J + \lambda \end{pmatrix}, \tag{4.55}$$

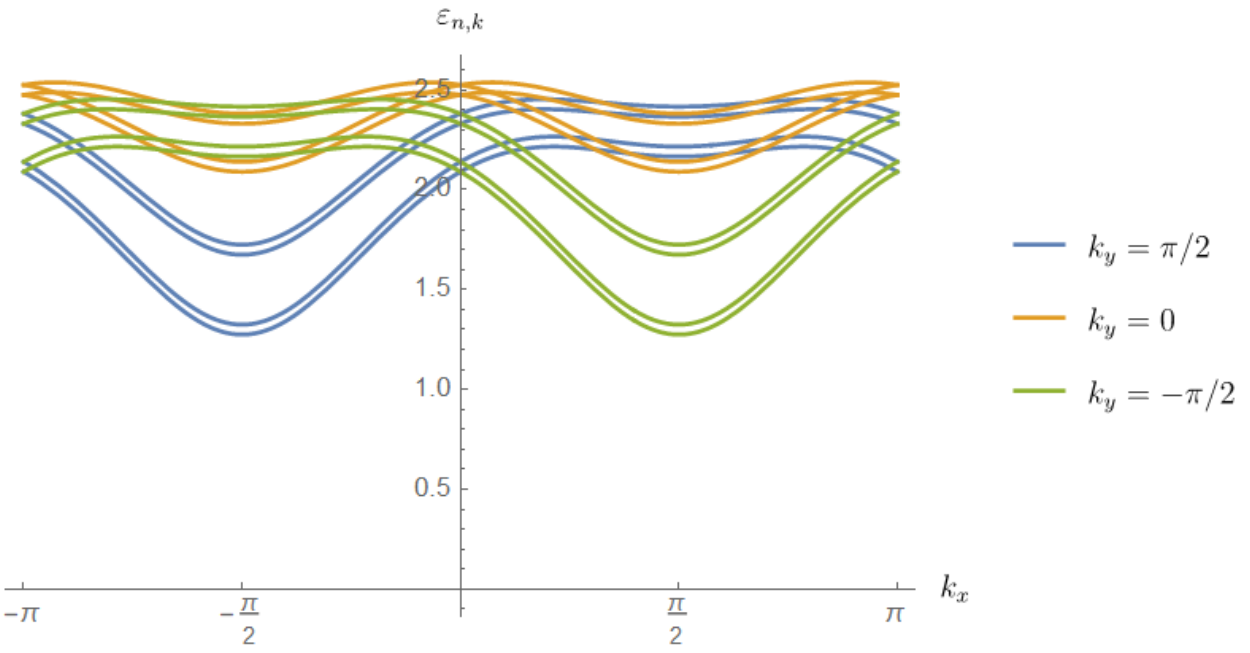

Figure 4.10: Slices of the spectrum, taking $A = 1$, $B = .1$, $\lambda = 6$, $B_z = .1$, $J = 1$, and $W_0 = 1$

and $S_1 \equiv \sin(k_x) - \sin(k_y)$ and $S_2 \equiv \sin(k_x) + \sin(k_y)$. We obtain the spectrum by diagonalizing the "dynamic matrix", given by $K = (\sigma_3 \otimes \mathbb{I}_2)M$. The results are shown for various values of W_0 and λ in Figures 4.10−4.14.

Next we wish to identify the critical behavior of the model. Therefore we must identify points in k space where there exists at least one zero eigenvalue. For small W_0, this exists at the points $k_0^{(0)} = (\pm\pi/2, \mp\pi/2)$. However for larger W_0, zero eigenvalues can occur at $k_0^{(1)} = \pm(\pi/2, \pi/2)$. To isolate these zero modes, we take the limit of vanishing magnetic field, take $J = +1$, and solve algebraically for the λ which yield zero energy eigenvalues:

$$\begin{aligned} k &= k_0^{(0)}, \qquad \lambda = J \pm 4J\sqrt{A^2 + B^2} \\ k &= k_0^{(1)}, \qquad \lambda = J \pm 2W_0\sqrt{A^2 + B^2} \end{aligned} \tag{4.56}$$

Examining the spectra at these points, we note that as B (corresponding to the ferromagnetic contribution) is tuned down to zero, the spectrum becomes linear. This is in agreement with the spin wave spectrum of antiferromagnetic chains. Furthermore, for $W_0 \geq 2J$, and

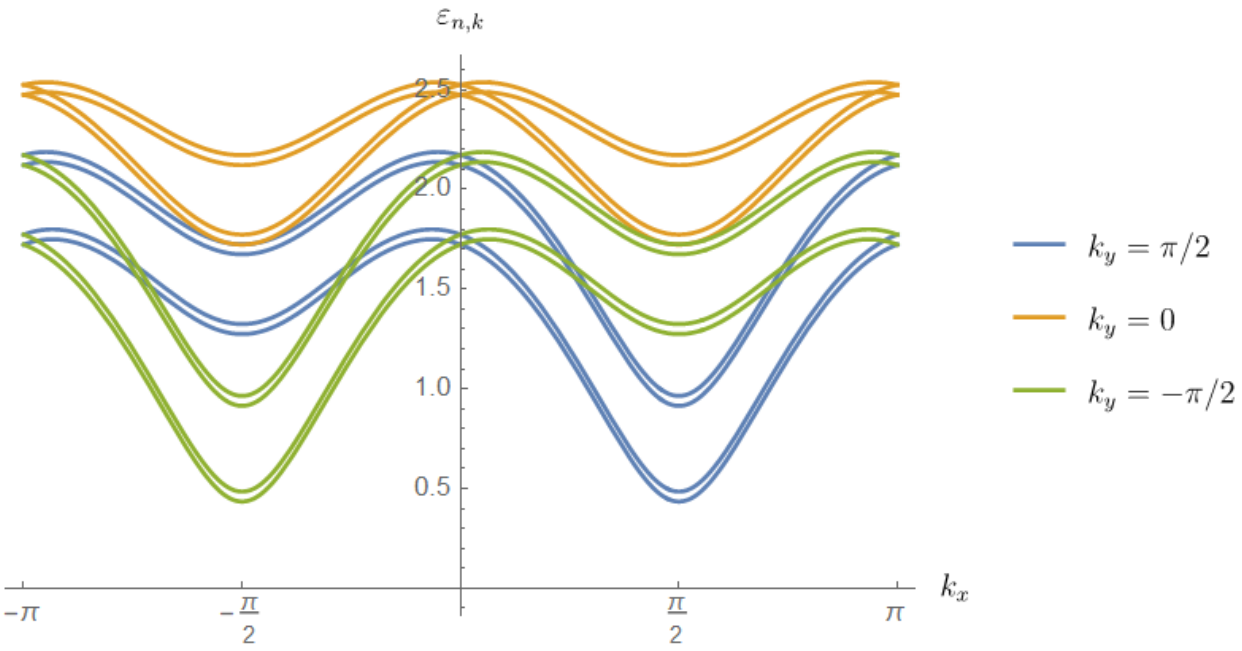

Figure 4.11: Slices of the spectrum, taking $A = 1$, $B = .1$, $\lambda = 6$, $B_z = .1$, $J = 1$, and $W_0 = 2.4$. Increasing the magnitude of W_0 changes the locations of the minima from $(\pm\pi/2, \mp\pi/2)$ to $\pm(\pi/2, \pi/2)$.

setting $\lambda = J - 2W_0\sqrt{A^2 + B^2}$, we are able to obtain another meaningful zero mode at $k_0^{(1)}$–indicating multicriticality.

4.5 Discussion

We have shown that a triplet density wave state induces a DM interaction in the host spin system. Although it has been shown that the triplet-singlet density wave state produces a nonzero thermal Hall effect[LL19], the magnitude of the experimentally-measured thermal Hall effect exceeds the maximum possible contribution from the density wave state alone by almost an order of magnitude.[LL19] The excitations of a spin system including DM interactions can, in principle, contribute to the thermal Hall conductivity[SCS19, HPL19, KH19]; however, we have shown the particular form of DM interaction generated by the triplet density wave does not seem to produce a nonzero κ_{xy}, and thus no additional contribution can be found through the influence of the density wave state on the underlying spin system.

The density wave can lead to other interesting effects in its host spin system. In particular, we have identified a critical density wave strength W_0^* for both ferromagnetic and antiferromagnetic backgrounds below which the ground state canting angle θ is independent of W_0, and above which θ grows with W_0. This transition is accompanied by a sharp decline in the spin-wave stiffness in the ferromagnet. In the antiferromagnet, at a particular density wave strength $\widetilde{W_0}$, we find a doubling of the number of zero modes, indicating multicriticality. Triplet-singlet density wave order is notoriously difficult to detect directly[HRC11], and so it is important to explore possible influences that the state might have on its host system. Experimental detection of such features could help to assess the importance of the triplet-singlet DDW state in the description of the pseudogap phase of the cuprates.

In our discussion of the antiferromagnet, we made the choice of taking the zero-flux ansatz, as a realistic mean-field state smoothly connected to the Neel state, and ignored the possible π-flux ansatz. It would be interesting in future work to include an analysis using the π-flux ansatz, and to investigate a possible crossover between these two ansatze as the

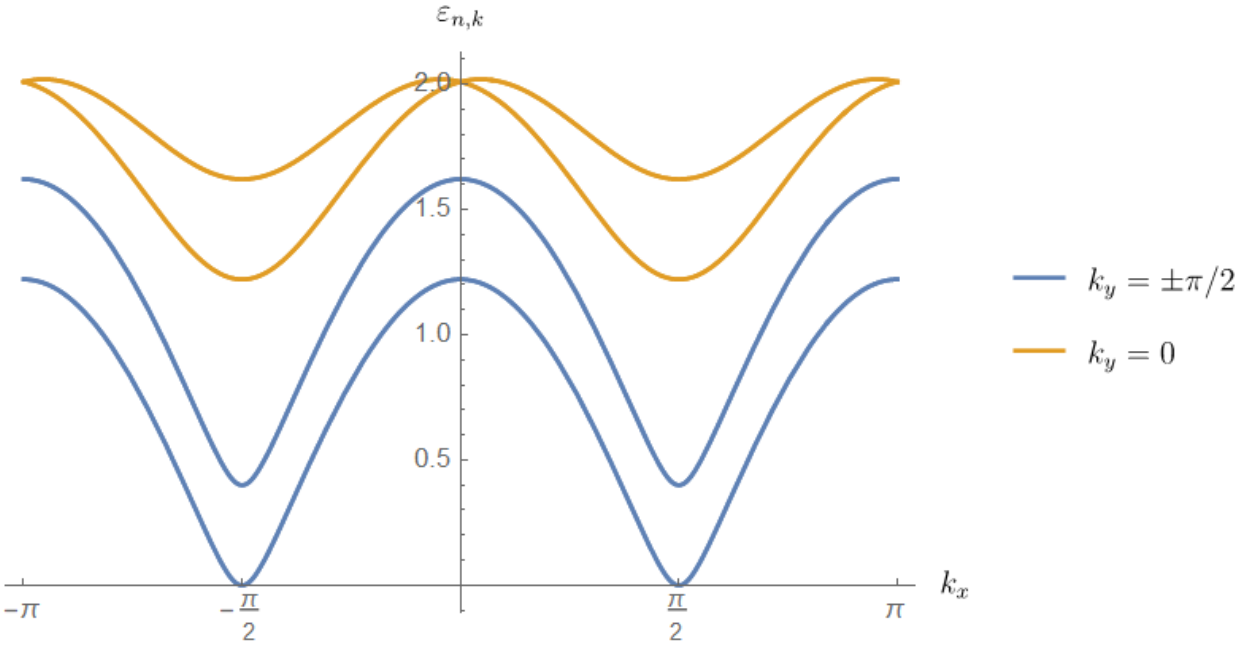

Figure 4.12: Slices of the spectrum, taking $A = 1$, $B = .1$, $\lambda = 1 - 4\sqrt{A^2 + B^2}$, $B_z = 0$, $J = 1$, and $W_0 = 2$. At $W_0 \geq 2$ we can obtain magnetic order corresponding to $k_0^{(1)}$

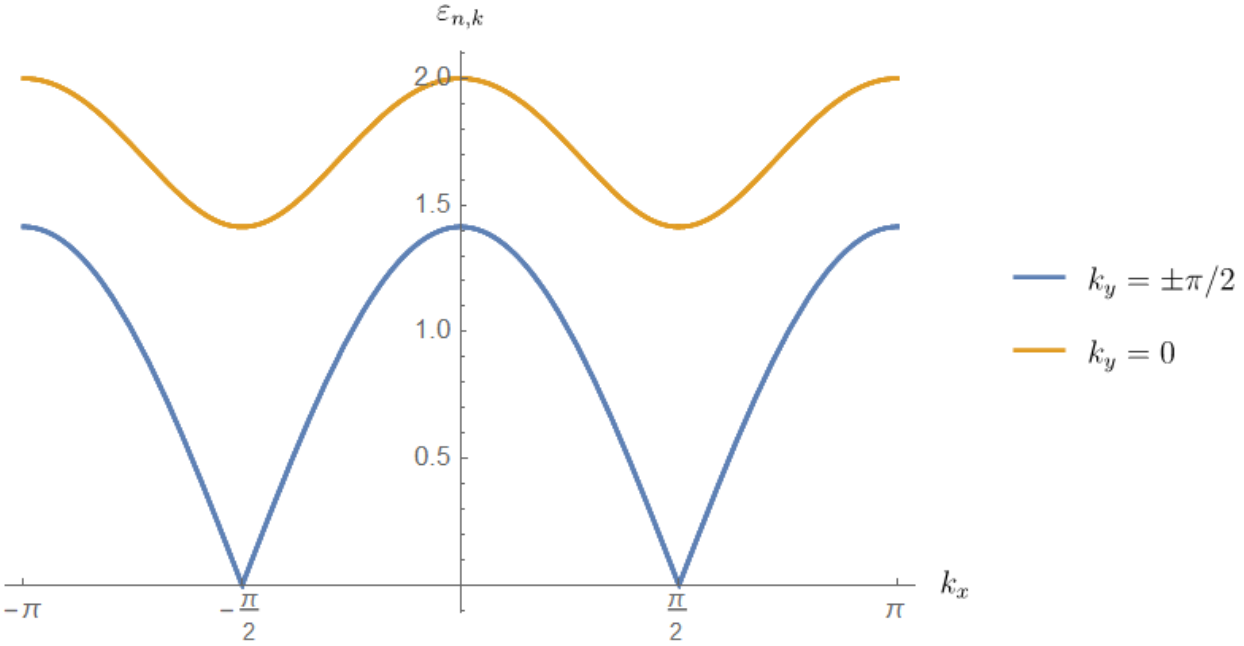

Figure 4.13: Slices of the spectrum, taking $A = 1$, $B = .1$, $\lambda = 1 - 4\sqrt{A^2 + B^2}$, $B_z = 0$, $J = 1$, and $W_0 = 2$. Setting $B = 0$ gives a linear spectrum.

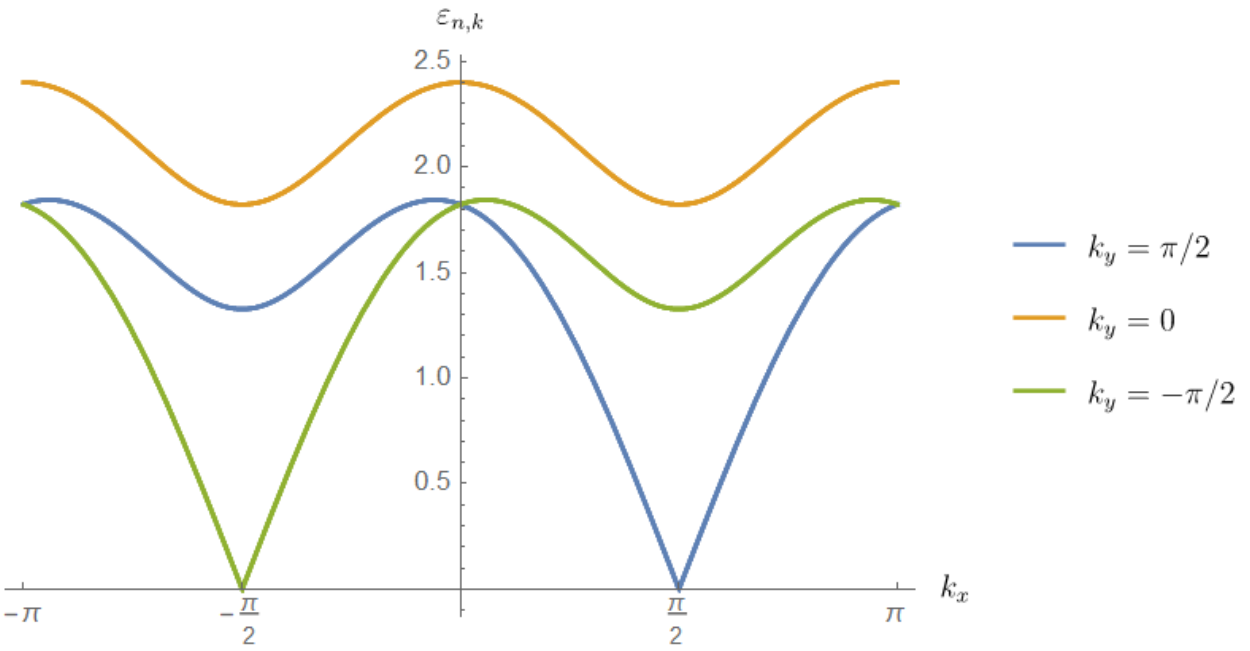

Figure 4.14: Slices of the spectrum, taking $A = 1$, $B = .1$, $\lambda = 1 - 2W_0\sqrt{A^2 + B^2}$, $B_z = .1$, $J = 1$, and $W_0 = 2.4$. Increasing W_0 allows for zero modes solely at $k_0^{(1)}$.

density-wave strength is varied.

[BCS57] J Bardeen, L N Cooper, and J R Schrieffer. "Theory of Superconductivity." *Phys. Rev.*, **108**(5):1175–1204, December 1957.

[BM89] J G Bednorz and KA Müller. "Possible High T_c superconductivity in the Ba-La-Cu-O system." *Z. Phys. B: Condens. Matter Matter*, **64**(189), 1989.

[Bon99] N E Bonesteel. "Singular Pair Breaking in the Composite Fermi Liquid Description of the Half-Filled Landau Level." *Physical Review Letters*, **82**(5):984–987, February 1999.

[CK08] Sudip Chakravarty and Hae-Young Kee. "Fermi pockets and quantum oscillations of the Hall coefficient in high-temperature superconductors." *Proceedings of the National Academy of Sciences*, **105**(26):8835–8839, July 2008.

[CLM01] Sudip Chakravarty, R B Laughlin, Dirk K Morr, and Chetan Nayak. "Hidden order in the cuprates." *Physical Review B*, **63**(9):116–10, January 2001.

[CNS95] Sudip Chakravarty, Richard E Norton, and Olav F Syljuåsen. *Phys. Rev. Lett.*, **74**, 1995.

[CRZ91] D Coffey, T M Rice, and F C Zhang. "Dzyaloshinskii-Moriya interaction in the cuprates." *Physical Review B*, **44**(18):10112–10116, November 1991.

[CS98] S Curnoe and P C E Stamp. "Quantum Oscillations of Electrons and of Composite Fermions in Two Dimensions: Beyond the Luttinger Expansion." *Physical Review Letters*, **80**(15):3312–3315, April 1998.

[CTF89] S W Cheong, J D Thompson, and Z Fisk. "Metamagnetism in La_2CuO_4." *Physical Review B*, **39**(7):4395–4398, March 1989.

[CTV06] Davide Ceresoli, T Thonhauser, David Vanderbilt, and R Resta. "Orbital magnetization in crystalline solids: Multi-band insulators, Chern insulators, and metals." *Physical Review B*, **74**(2):024408–13, July 2006.

[DCL10] R Daou, J Chang, David LeBoeuf, Olivier Cyr-Choinière, Francis Laliberté, Nicolas Doiron-Leyraud, B J Ramshaw, Ruixing Liang, D A Bonn, W N Hardy, and Louis Taillefer. "Broken rotational symmetry in the pseudogap phase of a high-Tc superconductor." *Nature*, pp. 1–4, January 2010.

[DPL07] Nicolas Doiron-Leyraud, Cyril Proust, David LeBoeuf, Julien Levallois, Jean-Baptiste Bonnemaison, Ruixing Liang, D A Bonn, W N Hardy, and Louis Taillefer. "Quantum oscillations and the Fermi surface in an underdoped high-Tc superconductor." *Nature*, **447**(7144):565–568, May 2007.

[DST94] R R Du, H L Stormer, D C Tsui, A S Yeh, L N Pfeiffer, and K W West. "Drastic Enhancement of Composite Fermion Mass near Landau Level Filling ν=1/2." *Physical Review Letters*, **73**(24):3274–3277, 1994.

[Fis04] R S Fishman. "Double exchange in a magnetically frustrated system." *Journal of Physics: Condensed Matter*, **16**(30):5483–5501, July 2004.

[GLB19] G Grissonnanche, A Legros, S Badoux, E Lefrançois, V Zatko, M Lizaire, F Laliberté, A Gourgout, J S Zhou, S Pyon, T Takayama, H Takagi, S Ono, N Doiron-Leyraud, and L Taillefer. "Giant thermal Hall conductivity in the pseudogap phase of cuprate superconductors." *Nature Publishing Group*, pp. 1–13, July 2019.

[GWW92] Martin Greiter, X G Wen, and Frank Wilczek. "Paired Hall states." *Nucl. Phys.*, **B374**(3):567–614, 1992.

[GZM16] Scott D Geraedts, Michael P Zaletel, Roger S K Mong, Max A Metlitski, Ashvin Vishwanath, and Olexei I Motrunich. "The half-filled Landau level: The case for Dirac composite fermions." *Science*, **352**(6282):197–201, April 2016.

[HAN03] N E Hussey, M Abdel-Jawad, A Carrington Nature, and 2003. "A coherent three-dimensional Fermi surface in a high-transition-temperature superconductor." *Nature*, **425**:814–817, October 2003.

[HF09] J T Haraldsen and R S Fishman. "Spin rotation technique for non-collinear magnetic systems: application to the generalized Villain model." *Journal of Physics: Condensed Matter*, **21**(21):216001–12, April 2009.

[HLR93] Bertrand I Halperin, Patrick A Lee, and Nicholas Read. "Theory of the half-filled Landau level." *Physical Review B*, 1993.

[HM95] Masahiko Hatatani and Toru Moriya. "Ferromagnetic Spin Fluctuations in Two-Dimensional Metals." *Journal of the Physical Society of Japan*, **64**(9):3434–3441, September 1995.

[HNP73] T Holstein, R E Norton, and P Pincus. "de Haas-van Alphen Effect and the Specific Heat of an Electron Gas." *Phys. Rev.*, **B8**(6):2649–2656, 1973.

[HPL19] Jung Hoon Han, Jin-Hong Park, and Patrick A Lee. "Consideration of thermal Hall effect in undoped cuprates." *Physical Review B*, **99**(20):1–10, May 2019.

[HRC11] Chen-Hsuan Hsu, S Raghu, and Sudip Chakravarty. "Topological density wave states of nonzero angular momentum." *Physical Review B*, **84**(15):155111–6, October 2011.

[Jai89] J K Jain. "Composite fermion approach for the fractional quantum Hall effect." *Physical Review Letters*, **63**(2):199–202, 1989.

[JSI89] H W Jiang, H L Stormer, D C Isui, L N Pfeiffer, and K W West. "Transport anomalies in the lowest Landau level of two-dimensional electrons at half-filling." *Physical Review B*, **40**(17):12013–12016, December 1989.

[KAS18] Koshi Kurashima, Tadashi Adachi, Kensuke M Suzuki, Yasushi Fukunaga, Takayuki Kawamata, Takashi Noji, Hitoshi Miyasaka, Isao Watanabe, Masanori Miyazaki, Akihiro Koda, Ryosuke Kadono, and Yoji Koike. "Development of Ferromagnetic Fluctuations in Heavily Overdoped $(Bi,Pb)_2Sr_2CuO_{6+\delta}$ Copper Oxides." *Physical Review Letters*, **121**(5):057002, July 2018.

[KDP80] K von Klitzing, G Dorda, and M Pepper. "New Method for High-Accuracy Determination of the Fine-Structure Constant Based on Quantized Hall Resistance." *Physical Review Letters*, **45**(6):494–497, August 1980.

[KGC07] Angela Kopp, Amit Ghosal, and Sudip Chakravarty. "Competing ferromagnetism in high-temperature copper oxide superconductors." *Proceedings of the National Academy of Sciences*, **104**(15):6123–6127, April 2007.

[KH19] Masataka Kawano and Chisa Hotta. "Thermal Hall effect and topological edge states in a square-lattice antiferromagnet." pp. 1–16, February 2019.

[KK03] A P Kampf and A A Katanin. "Competing phases in the extended U-V-J Hubbard model near the Van Hove fillings." *Physical Review B*, **67**(12):4126–14, March 2003.

[KKA16] Toru Kikuchi, Takashi Koretsune, Ryotaro Arita, and Gen Tatara. "Dzyaloshinskii-Moriya Interaction as a Consequence of a Doppler Shift due to Spin-Orbit-Induced Intrinsic Spin Current." *Physical Review Letters*, **116**(24):247201–6, June 2016.

[KKM10] M I Katsnelson, Y O Kvashnin, V V Mazurenko, and A I Lichtenstein. "Correlated band theory of spin and orbital contributions to Dzyaloshinskii-Moriya interactions." *Physical Review B*, **82**(10):100403–4, September 2010.

[KMR19] Prashant Kumar, Michael Mulligan, and S Raghu. "Emergent reflection symmetry from nonrelativistic composite fermions." pp. 1–5, May 2019.

[KMT15] Shamit Kachru, Michael Mulligan, Gonzalo Torroba, and Huajia Wang. "Mirror symmetry and the half-filled Landau level." *Physical Review B*, **92**(23):235105–16, December 2015.

[KRM19] Prashant Kumar, S Raghu, and Michael Mulligan. "Composite fermion Hall conductivity and the half-filled Landau level." pp. 1–7, June 2019.

[KS00] A Kolodziejczyk and J Spalek. "Spin fluctuations in a very weak itinerant ferromagnet: Y_4Co_3." *Journal of Physics F: Metal Physics*, **14**(5):1277–1289, November 2000.

[KSM91] Y Kubo, Y Shimakawa, T Manako, and H Igarashi. "Transport and magnetic properties of $Tl_2Ba_2CuO_{6+\delta}$ showing a δ-dependent gradual transition from an 85-K superconductor to a nonsuperconducting metal." *Physical Review B*, **43**(10):7875–7882, April 1991.

[Lau83] R B Laughlin. "Anomalous quantum Hall effect: An Incompressible quantum fluid with fractionally charged excitations." *Physical Review Letters*, **50**(18):1395–1398, 1983.

[Lau14] R B Laughlin. "Hartree-Fock computation of the high-Tc cuprate phase diagram." *Physical Review B*, **89**(3):035134–19, January 2014.

[LL19] Zi-Xiang Li and Dung-Hai Lee. "The thermal Hall conductance of two doped symmetry-breaking topological insulators." *arXiv.org*, May 2019.

[LNW06] Patrick A Lee, Naoto Nagaosa, and Xiao-Gang Wen. "Doping a Mott insulator: Physics of high-temperature superconductivity." *Rev. Mod. Phys.*, **78**(1):17–85, January 2006.

[LS17] Michael Levin and Dam Thanh Son. "Particle-hole symmetry and electromagnetic response of a half-filled Landau level." *Physical Review B*, **95**(12):125120–8, March 2017.

[Lut60] J M Luttinger. "Fermi Surface and Some Simple Equilibrium Properties of a System of Interacting Fermions." *Phys. Rev.*, **119**(4):1153–1163, 1960.

[LW07] Edwin Langmann and Mats Wallin. "Mean Field Magnetic Phase Diagrams for the Two Dimensional t - t' - U Hubbard Model." *Journal of Statistical Physics*, **127**(4):825–840, March 2007.

[Mat81] D C Mattis. *The Theory of Magnetism I: Statics and Dynamics*. Springer-Verlag Berlin Heidelberg, 1981.

[MK73] Toru Moriya and Arisato Kawabata. "Effect of Spin Fluctuations on Itinerant Electron Ferromagnetism." *Journal of the Physical Society of Japan*, **34**(3):639–651, March 1973.

[MLM13] L Messio, C Lhuillier, and G Misguich. "Time reversal symmetry breaking chiral spin liquids: Projective symmetry group approach of bosonic mean-field theories." *Physical Review B*, **87**(12), March 2013.

[MSS01] V A Miransky, G W Semenoff, I A Shovkovy, and L C R Wijewardhana. "Color superconductivity and nondecoupling phenomena in (2+1)-dimensional QCD." *Phys. Rev. D*, **64**(2):390–10, June 2001.

[Nag66] Yosuke Nagaoka. "Ferromagnetism in a Narrow, Almost Half-Filled s Band." *Phys. Rev.*, **147**(1):392–405, 1966.

[Nay00] Chetan Nayak. "Density-wave states of nonzero angular momentum." *Physical Review B*, **62**(8):4880–4889, August 2000.

[NBM03] S Nakamae, K Behnia, N Mangkorntong, M Nohara, H Takagi, S J C Yates, and N E Hussey. "Electronic ground state of heavily overdoped nonsuperconducting $La_{2-x}Sr_xCuO_4$." *Physical Review B*, **68**(10):468–4, September 2003.

[NJK99] A A Nersesyan, G I Japaridze, and I G Kimeridze. "Low-temperature magnetic properties of a two-dimensional spin nematic state." *Journal of Physics: Condensed Matter*, **3**(19):3353–3366, January 1999.

[NOM94] T Nakano, M Oda, C Manabe, N Momono, Y Miura, and M Ido. "Magnetic properties and electronic conduction of superconducting $La_{2-x}Sr_xCuO_4$." *Physical Review B*, **49**(22):16000–16008, June 1994.

[NPK07] M R Norman, D Pines, and C Kallin. "The pseudogap: friend or foe of high Tc?" *Advances in Physics*, **54**(8):715–733, February 2007.

[ONK91] M Oda, T Nakano, Y Kamada, and M Ido. "Electronic states of doped holes and magnetic properties in $La_{2-x}M_xCuO_4$ (M = Sr, Ba)." *Physica C: Superconductivity*, **183**(4-6):234–240, November 1991.

[PBH02] Cyril Proust, Etienne Boaknin, R W Hill, Louis Taillefer, and A P Mackenzie. "Heat Transport in a Strongly Overdoped Cuprate: Fermi Liquid and a Pure d-Wave BCS Superconductor." *Physical Review Letters*, **89**(14):1196–4, September 2002.

[PKB17] W Pan, W Kang, K W Baldwin, K W West, L N Pfeiffer, and D C Tsui. "Berry phase and anomalous transport of the composite fermions at the half-filled Landau level." *Nature Physics*, **13**(12):1168–1172, August 2017.

[PTG82] M A Paalanen, D C Tsui, and A C Gossard. "Quantized Hall effect at low temperatures." *Physical Review B*, **25**(8):5566–5569, April 1982.

[RC19] Nicholas Rombes and Sudip Chakravarty. "Specific heat and pairing of Dirac composite fermions in the half-filled Landau level." *Annals of Physics*, **409**:167915, October 2019.

[Sch89] H J Schulz. "Fermi-surface instabilities of a generalized two-dimensional Hubbard model." *Physical Review B*, **39**(4):2940–2943, February 1989.

[SCS19] Rhine Samajdar, Shubhayu Chatterjee, Subir Sachdev, and Mathias S Scheurer. "Thermal Hall effect in square-lattice spin liquids: A Schwinger boson mean-field study." *Physical Review B*, **99**(16):165126, April 2019.

[SHP08] Suchitra E Sebastian, N Harrison, E Palm, T P Murphy, C H Mielke, Ruixing Liang, D A Bonn, W N Hardy, and G G Lonzarich. "A multi-component Fermi surface in the vortex state of an underdoped high-Tc superconductor." *Nature*, **454**(7201):200–203, July 2008.

[SKP10] J E Sonier, C V Kaiser, V Pacradouni, S A Sabok-Sayr, C Cochrane, D E MacLaughlin, S Komiya, and N E Hussey. "Direct search for a ferromagnetic phase in a heavily overdoped nonsuperconducting copper oxide." *Proceedings of the National Acadamy of Sciences*, **107**(40):17131–17134, October 2010.

[SMM13] Ryuichi Shindou, Ryo Matsumoto, Shuichi Murakami, and Jun-ichiro Ohe. "Topological chiral magnonic edge mode in a magnonic crystal." *Physical Review B*, **87**(17):174427–11, May 2013.

[Son15] Dam Thanh Son. "Is the Composite Fermion a Dirac Particle?" *Physical Review X*, **5**(3):031027–14, September 2015.

[SWZ20] Tarapada Sarkar, D S Wei, J Zhang, N R Poniatowski, P R Mandal, A Kapitulnik, and Richard L Greene. "Ferromagnetic order beyond the superconducting dome in a cuprate superconductor." *Science*, **368**(6490):532–534, May 2020.

[TA94] Tineke Thio and Amnon Aharony. "Weak Ferromagnetism and Tricriticality in Pure La_2CuO_4." *Physical Review Letters*, **73**(6):894–897, August 1994.

[Tat19] Gen Tatara. "Effective gauge field theory of spintronics." *Physica E: Low-dimensional Systems and Nanostructures*, **106**:208–238, February 2019.

[THM92] I Terasaki, M Hase, A Maeda, K Uchinokura, T Kimura, K Kishio, I Tanaka, and H Kojima. "Doping effects on the anisotropic magnetic susceptibility in single-crystal $La_{2-x}Sr_xCuO_4$." *Physica C: Superconductivity*, **193**(3-4):365–370, April 1992.

[TII89] H Takagi, T Ido, S Ishibashi, M Uota, S Uchida, and Y Tokura. "Superconductor-to-nonsuperconductor transition in $(La_{1-x}Sr_x)_2CuO_4$ as investigated by transport and magnetic measurements." *Physical Review B*, **40**(4):2254–2261, August 1989.

[TSG82] D C Tsui, H L Stormer, and A C Gossard. "Two-dimensional magnetotransport in the extreme quantum limit." *Physical Review Letters*, **48**(22):1559–1562, 1982.

[UM75] Kazuo Ueda and Toru Moriya. "Contribution of Spin Fluctuations to the Electrical and Thermal Resistivities of Weakly and Nearly Ferromagnetic Metals." *Journal of the Physical Society of Japan*, **39**(3):605–615, September 1975.

[Var99] C M Varma. "Pseudogap Phase and the Quantum-Critical Point in Copper-Oxide Metals." *Physical Review Letters*, **83**(17):3538–3541, October 1999.

[Var06] C M Varma. "Theory of the pseudogap state of the cuprates." *Physical Review B*, **73**(15):53–17, April 2006.

[WBK05] S Wakimoto, R J Birgeneau, A Kagedan, Hyunkyung Kim, I Swainson, K Yamada, and H Zhang. "Magnetic properties of the overdoped superconductor $La_{2-x}Sr_xCuO_4$ with and without Zn impurities." *Physical Review B*, **72**(6):2833–9, August 2005.

[WC16a] Zhiqiang Wang and Sudip Chakravarty. "Onsager rule, quantum oscillation frequencies, and the density of states in the mixed-vortex state of cuprates." *Physical Review B*, **93**(18):184505, May 2016.

[WC16b] Zhiqiang Wang and Sudip Chakravarty. "Pairing of particle-hole symmetric composite fermions in half-filled Landau level." *Physical Review B*, **94**(16):165138–7, October 2016.

[WCH17] Chong Wang, Nigel R Cooper, Bertrand I Halperin, and Ady Stern. "Particle-Hole Symmetry in the Fermion-Chern-Simons and Dirac Descriptions of a Half-Filled Landau Level." *Physical Review X*, **7**(3):590–21, August 2017.

[WES87] R Willett, J P Eisenstein, H L Stormer, D C Tsui, A C Gossard, and J H English. "Observation of an even-denominator quantum number in the fractional quantum Hall effect." *Physical Review Letters*, **59**(15):1776–1779, 1987.

[WMC14] Zhiqiang Wang, Ipsita Mandal, Suk Bum Chung, and Sudip Chakravarty. "Pairing in half-filled Landau level." *Annals Phys.*, **351**:727–738, 2014.

[WPR90] R L Willett, M A Paalanen, R R Ruel, K W West, L N Pfeiffer, and D J Bishop. "Anomalous sound propagation at ν=1/2 in a 2D electron gas: Observation of a spontaneously broken translational symmetry?" *Physical Review Letters*, **65**(1):112–115, July 1990.

[XSD08] Jing Xia, Elizabeth Schemm, G Deutscher, S A Kivelson, D A Bonn, W N Hardy, R Liang, W Siemons, G Koster, M M Fejer, and A Kapitulnik. "Polar Kerr-Effect Measurements of the High-Temperature $YBa_2Cu_3O_{6+x}$ Superconductor: Evidence for Broken Symmetry near the Pseudogap Temperature." *Physical Review Letters*, **100**(12):127002–4, March 2008.

[YRZ06] Kai-Yu Yang, T M Rice, and Fu-Chun Zhang. "Phenomenological theory of the pseudogap state." *Physical Review B*, **73**(17):R755–10, May 2006.

[YW16] Xu Yang and Fa Wang. "Schwinger boson spin-liquid states on square lattice." *Physical Review B*, **94**(3):1–25, July 2016.

[ZBL16] L Zhao, C A Belvin, R Liang, D A Bonn, W N Hardy, N P Armitage, and D Hsieh. "A global inversion-symmetry-broken phase inside the pseudogap region of YBa2Cu3Oy." *Nature Physics*, **13**(3):250–254, November 2016.